國 立 交 通 大 學

電信工程學系碩士班

碩 士 論 文

具有處理能力的衛星轉頻器之架構與效能

Architecture and Performance of a Satellite Transponder with On-Board Processing Capability

研 究 生：廖明堃

指導教授：蘇育德 博士

中 華 民 國 九 十 五 年 七 月

具有處理能力的衛星轉頻器之架構與效能

Architecture and Performance of a Satellite Transponder with On-Board Processing Capability

研 究 生 : 廖明堃　　Student : Ming-Kun Liao

指導教授 : 蘇育德 博士　　Advisor : Dr. Yu T. Su

國 立 交 通 大 學

電 信 工 程 學 系 碩 士 班

碩 士 論 文

A Thesis

Submitted to Department of Communication Engineering

College of Electrical and Computer Engineering

National Chiao Tung University

in Partial Fulfillment of the Requirements

for the Degree of

Master of Science

in

Communication Engineering

July 2006

Hsinchu, Taiwan, Republic of China

中華民國九十五年七月

具有處理能力的衛星轉頻器之架構與效能

研究生：廖明堃　　指導教授：蘇育德 博士

國立交通大學電信工程學系碩士班

中文摘要

本論文探討具抗干擾(anti-jam, AJ)能力的衛星轉頻器之架構及效能。我們所考慮的上傳鏈路(uplink)除有加成性的白高斯背景雜訊(AWGN)另有惡意的干擾，即所謂的部份頻寬雜訊干擾(partial-band noise jamming)。我們發現具有處理(processing)或再生(regenerative)功能之衛星轉頻器可以提供強大的抗干擾能力。為強化抗干擾能力我們使用了慢跳頻式的差分相位相移鍵信號並加上了渦輪編碼。

經過差分相位相移鍵調變的渦輪編碼信號可視為等同於一個串聯編碼架構，其中內部碼(inner code)為碼率為一的特殊迴旋碼而外部碼(outer code)則為渦輪碼。基於此種等效模式，我們提出一種迭代的解碼結構並且藉由數值的模擬檢驗此種不同於以往的解碼排程的效率。我們更進一步使用塊間重排(IBP)的渦輪碼使得在解碼時可藉由迭代交換不同區塊之間的解碼訊息以有效的更正錯誤。實驗數值證實這種改錯碼能夠在跳頻速率很低時仍維持相當良好的性能。另一方面，傳統的渦輪碼需有較高的跳頻速率方能滿足系統的抗干擾能力性能要求。

Architecture and Performance of a Satellite Transponder with On-Board Processing Capability

Student : Ming-Kun Liao Advisor : Yu T. Su

Department of Communications Engineering

National Chiao Tung University

Abstract

We consider a secure satellite link in which a slow frequency-hopped (FH), turbo-coded DPSK signal is used in the uplink. Several detector structures are proposed and both processing and bent-pipe transponders are considered although our emphasis is on the former class. Regarding the turbo-coded DPSK signal as an equivalent serially concatenated coding scheme with the inner code being the rate-1 DPSK encoder, we propose an iterative decoder architecture and examine the effectiveness of different decoding schedules. We also consider two interleaver structures for the corresponding turbo codes. The first one is a conventional block oriented interleaver while the second one is the so-called inter-block permutation (IBP) interleaver. Numerical results indicate that sufficient AJ margin is achievable with the proposed signal waveform and decoding scheme. Furthermore, the IBP-interleaved turbo coded system offer additional tradeoff between hopping rate and performance. It offers sufficient AJ capability even the FH rate is relatively low.

Contents

List of Figures

Chapter 1

Introduction

Anti-jamming (AJ) capability is the most critical measure and requirement of a military communication system. In general, AJ strategies are built upon the following technologies: 1) wideband transmission, 2) multiple antennas (i.e. antenna array), 3) robust modulation, and 4) forward error-correcting (FEC) codes. Spread spectrum (SS) techniques belong to the first category and frequency-hopping (FH) is generally considered as a more robust and efficient electronic counter counter-measure (ECCM) scheme than the direct sequence spread spectrum (DSSS) waveform. In conjunction with FHSS waveform, one can use either differential phase shift keying (DPSK) [1] or M-ary phase shift keying (MFSK) to enhance the system's AJ robustness, as these two modulation schemes can be incoherently detected and is thus immune to phase noise.

To further improve a ECCM system's AJ capability, one can invoke a powerful FEC coding scheme. In particular, turbo codes, which form a class of very powerful FEC codes [2], have been shown to be effective in meeting the AJ requirement [3, 4]. It has been shown in [11] that a turbo coded system is not sensitive to the mismatch of SNR if the BPSK modulation is used. However, whether this conclusion is valid when the DPSK or MFSK modulation is used remains unanswered. Hence, the robustness of DPSK and MFSK in the presence of phase error should assessed against their SNR sensitivity. In light of such a concern, we need to find a reliable SNR estimation scheme to avoid performance degradation.

The purpose of this thesis is to propose and validate solutions to some critical system issues concerning the design of a turbo-coded FHSS DPSK satellite link. Several new techniques are incorporated into the physical layer design. We use a inter-block permutation (IBP) turbo code, an improved DPSK detector, a very efficient signal to noise ratio (SNR) estimator, and an efficient iterative joint demodulation and decoding structure. As will be shown by numerical examples, the proposed system design makes possible for the overall satellite link to render a large enough AJ margin. The reasons for invoking these new techniques are given in the following paragraphs.

Although a differential coherent DPSK receiver is more robust it suffers from performance degradation with respect to a coherent detector. In [6], an infinite impulse response (IIR) filter with decision feedback equipped with a conventional differential detection circuit is proposed to improve the reference SNR. It was shown that the resulting DPSK performance comes very close to that of the coherent DPSK detector.

For turbo-coded DPSK system, we modify the structure of [6] to compensate for the received phase offset ϕ_0. We also replace the conventional DPSK demodulator by a soft-input soft-output (SISO) MAP DPSK detector whose output, after proper deinterleaving, is forwarded to a turbo decoder. We thus have a turbo coded DPSK receiver structure that is equivalent to that of an iterative decoder for a serial concatenated code first conceived by Forney [5]. This receiver structure will be referred to as IIR filtered (or IBP-) turbo DPSK detector.

It has been shown that the IBP turbo code (IBPTC) is an efficient high speed turbo code. However, the use of an IBP turbo code in a military communication system is motivated by another attractive feature of IBPTCs, i.e., an IBPTC decoder continuously expands its message-passing range as the number of decoding iterations increases. Note that in a channel that suffers from partial band jamming, the received samples consist of jammed (unreliable) and unjammed (reliable) samples. Increasing the iteration number thus enable the decoder to collect more reliable samples to help decoding unreliable bits.

The rest of this thesis is organized as follows. Chapter 2 presents the system and channel (jammer) model of a Ka-band satellite link. Various SNR estimation algorithms are discussed in Chapter 3 and the two key performance-enhancing technologies, i.e., IBP interleaving and IIR filter-aided DPSK detection are presented in the ensuing chapter. Chapter 5 gives numerical uplink performance for a regenerative link with various on-board receiving structures. We discuss the satellite nonlinear effect in Chapter 6 and provide end-to-end (overall link) performance in the following chapter. The last chapter summarizes our major results and compares the worst case performance of the proposed architectures.

Chapter 2

System and Channel Models

2.1 Turbo coded FH/DPSK systems

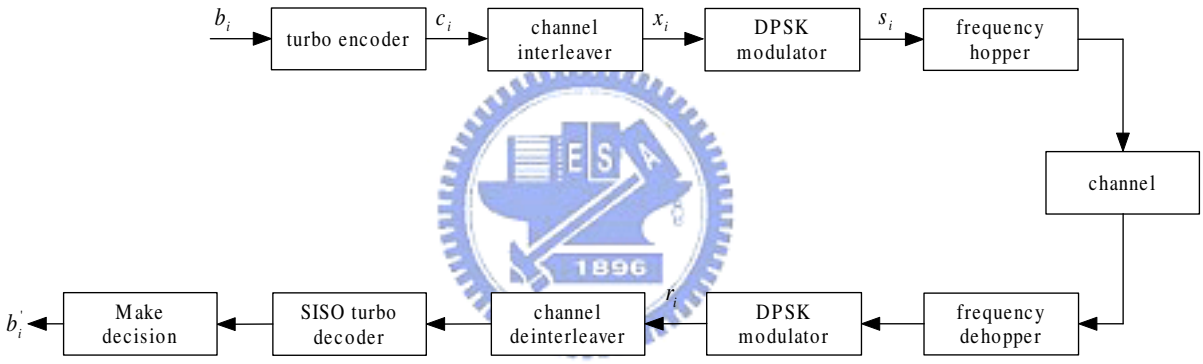

Figure 2.1: Block diagram of a turbo coded slow FH/DPSK system.

Shown in Fig. 2.1 is a block diagram of the turbo-coded DPSK digital satellite communication system. In the (ground) transmitter site, we have three main building blocks representing the turbo encoder, channel interleaver and DPSK modulator. A sequence of N_b information bits $\mathbf{b} = (b_1, b_2, \cdots, b_{N_b})$ is encoded by a rate $\frac{1}{3}$ turbo encoder without puncturing into a sequence of N coded bits $\mathbf{c} = (c_1, c_2, \cdots, c_N)$. Coded bit stream is then interleaved by the channel interleaver, denoted by π, through which $\mathbf{c}$ is written by columns and the interleaved sequence is read by rows. We represent the interleaving operation by $x_i = \pi(c_i)$. The DPSK modulator differentially encode the

interleaved sequence into the sequence $\mathbf{d} = (d_1, d_2, \cdots, d_N)$ and produce the bi-phase sequence, $\{s_i = e^{(j\phi_i)}\}$, where $\phi_i \in \{0, \pi\}$.

2.2 Frequency-hopped systems

In a frequency hopping (FH) system, the modulated carrier is hopped in a pseudo-random fashion. An FH system with a hopping rate larger than one hop per channel symbol is called a fast FH system; otherwise it is referred to as a slow FH system. Because the phase coherency among different hops is very difficult to maintain, coherent FH/DPSK systems remain only a theoretical interest. Our study considers a DPSK modulated slow hopping FHSS system. The phase continuity among adjacent samples of a slow FH system makes the DPSK modulated signals detectable. When we observe an FH/DPSK waveform over a number of hop periods, the its frequency content might span the entire spread spectrum bandwidth W_{ss}. Let R_b be the DPSK rate so that the SS band consists of $W_{ss}/R_b = N_{ss}$ subbands. In the absence of jamming and radio frequency interference (RFI) a satellite channel is often modelled as an additive white Gaussian noise (AWGN) channel. One can then express the baseband matched filter output at the ith subband as

$$r_i = \sqrt{E_s} e^{j(\phi_i + \phi_0)} + n_i. \tag{2.1}$$

where ϕ_0 is a random phase rotation with uniform distribution $U[0; 2\pi)$ and n_i is a zero mean complex Gaussian random variable.

It is reasonable to assume that the jammer does not have the knowledge of the hopping pattern but it does know the frequency band in which the signal was transmitted. A common approach for a jammer is to concentrate its limited power resource over a fraction of W_{ss} in the form of random noise or random tones. The former strategy is called a partial band noise jammer (PBNJ) while the later strategy is referred to as a multitone jammer (MTJ). Because the communicator in an FH system can in principle

avoid using certain frequency bands that it has detected as being jammed and changing its hopping pattern, the jammer should also varies its targeted band. For a worst case consideration, we assume that the jammer can modify its power distribution strategy, alter the jammed band over W_{ss}. But the rate of changes is slow relative to the FH dwell time $1/R_h = T_h$ and yet fast enough to deny the opportunity of the FH communicators to detect the location of jammed bands and to take necessary remedial action. We also assume that shifts in the jammed band are synchronous with the hop clock so that the communication channel is stationary during a hop period. Finally, we assume that during a given hop period, the band used by the modulated signals lies entirely inside or outside the jammed band.

2.3 Partial-band noise jammer

A PBNJ emits a fixed amount radiated power over a portion of the frequency hopping band W_{SS}, it distributes its total available power P_J over a band of W_J Hz band. The jammed band occupies a fraction $u = W_J/W_{SS}$ $(0 < u \leq 1)$ of the full spread spectrum (SS) bandwidth. For a perfect FHSS system, the probability that a transmitting band is jammed can be determined by an independent Bernoulli distribution with jamming probability u, i.e. a jammed subsequence on a given band is irrelevant to other subsequences. The equivalent power spectrum density (PSD) within the jammed band is

$$N_J^{'} = \frac{P_J}{W_J} = \frac{P_J/W_{SS}}{u} = \frac{N_J}{u}(W/Hz). \tag{2.2}$$

If a DPSK encoded sub-sequence is not jammed, the total noise PSD density level, N_t, is identical to that of AWGN N_0, i.e.,

$$SNR = \frac{E_s}{N_t} = \frac{E_s}{N_0} \tag{2.3}$$

where E_s is symbol energy. In case of a band is jammed, the total noise power corrupting the band is the sum of the background thermal noise power and the jammer's power,

i.e., the equivalent signal to noise plus jamming power ratio is given by

$$SNR = \frac{E_s}{N_t} = \frac{E_s}{N_0 + N_J'} = \frac{E_s}{N_0 + \frac{N_J}{u}}. \tag{2.4}$$

When the channel state is known, the receiver can classify the channel condition as the jammed and the un-jammed states. The previous independent Bernoulli distribution assumption shows that the probability of the jammed state is u while the probability of the unjammed state is $1 - u$. Note that knowing the channel state helps the receiver a lot in boosting its AJ performance and our simulation results show the fact.

2.4 Multitone jammer

Another jammer model which is more effective against FH waveforms is the multitone jammer (MTJ). This kind of jammer divide its total jamming power evenly among Q independent random tones that are uniformly distributed over all the candidate FH bands ($Q_t = W_{ss}/R_h$) within the whole SS band. We assume that the jammer know how the communicator partition the total hopping band into disjoint subbands and each jamming tone coincide with one of the Q_t available carrier frequencies. Thus a signal jammed at most one jamming tone per hopping period. We also assume that the multitone jammer can randomly rearrange the jamming tones locations to thwart any FH avoidance measures. And the time of the jammer to relocate the jamming tones is also assumed to be synchronous with the communicator's hopping clock. With these above assumptions the probability a signal is jammed by a MTJ is given by

$$\rho \equiv \frac{Q}{Q_t} \tag{2.5}$$

Let SJR be the signal-to-jammer power ratio and the power of each jamming tone is denoted as J_t,

$$SJR = \frac{S}{J} = \frac{signal\ power}{total\ jamming\ power}, \tag{2.6}$$

$$J_t = \frac{J}{Q} = \frac{total\ jamming\ power}{number\ of\ jamming\ tones}. \tag{2.7}$$

The signal-to-jamming tone power ratio SJR_t is given

$$SJR_t = \frac{S}{J_t} = \frac{S}{J/Q} = \frac{S}{J}(Q_t\rho) \tag{2.8}$$

$Q_t = W_{ss}/R_h \stackrel{def}{=} G$ is known as the processing gain.

2.5 AJ capability of an FH system

Figs. 2.3 and 2.2 show the AJ performance of a BPSK system when a conventional rate 1/3 convolutional turbo code (CTC) with two identical $\{15, 13\}$ component codes is used. We will use the same CTC component codes throughout our discussion. It is found that the AJ effectiveness improves as the hopping rate increases. If a fast hopping rate of 1 bit/hop is employed, the jammer is forced to distribute its power over the entire spread spectrum bandwidth while Fig. 2.2 indicates that if a much slower hopping rate 100 bits/hop is used full band jamming is optimal only if the jammer has enough power, i.e., $E_b/N_0 < 0.8$ dB. For a slow FH system with hopping rate = 100 hops/sec and date rate = 1 Gbits/sec, we have 100 bits/hop which will be used as the default hopping block size in all subsequent discussion unless otherwise specified.

The ultimate goal of an FH AJ system is to force the jammer to jam the entire SS band regardless of how much power it can emit. In other words, we hope to eliminate the jammer's degree of freedom in choosing which portion of W_{ss} for jamming.

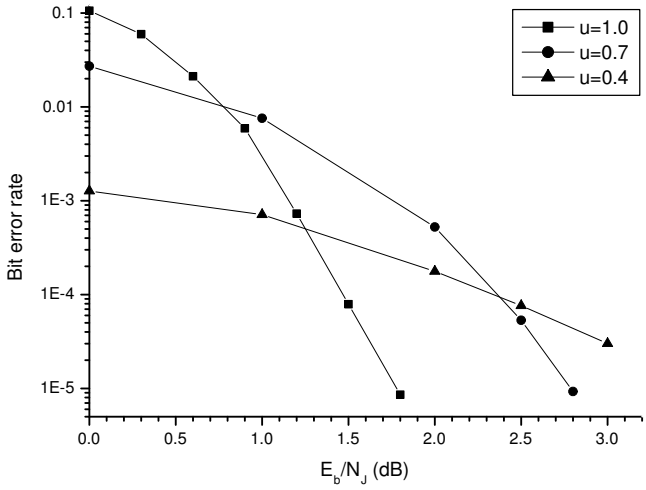

Figure 2.2: AJ performance of a turbo coded BPSK system with interleaver size 400, 100 bits/hop and $(E_b/N_0)_t = 15$ dB.

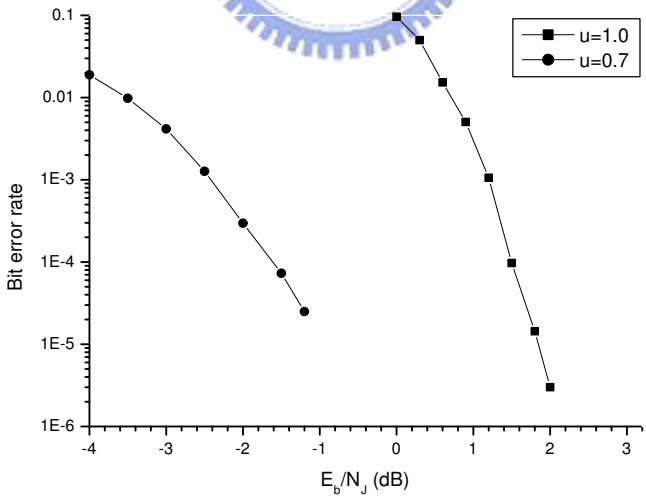

Figure 2.3: AJ performance of a turbo coded BPSK system with interleaver size 400, 1 bits/hop and $(E_b/N_0)_t = 15$ dB.

Chapter 3

Channel Estimation Schemes

3.1 Gaussian approximation and extrinsic information

It is well known that a turbo decoder needs to have good SNR estimate, as it represents the channel information in computing the reliability of an information bit. For a BPSK signal transmitted over an AWGN channel, the corresponding received matched filter output is given by

$$r_i = \sqrt{E_s} x_i + n_i \tag{3.1}$$

where $x_i = +1$ if $b_i = 0$, $x_i = -1$ if $b_i = 1$ and $n_i \sim N\left(0, \frac{N_0}{2}\right)$. Then

$$\begin{aligned} L\left(b_i|r_i\right) &= \ln \frac{p(r_i|b_i=0)\cdot P(b_i=0)}{p(r_i|b_i=1)\cdot P(b_i=1)} \\ &= \ln \frac{\exp\left(-\frac{E_s}{N_0}(r_i-1)^2\right)}{\exp\left(-\frac{E_s}{N_0}(r_i+1)^2\right)} + \ln \frac{P(b_i=0)}{P(b_i=1)} \\ &= 4\cdot\frac{E_s}{N_0}\cdot r_i + L(b_i) \\ &= L_c \cdot r_i + L(b_i) \end{aligned} \tag{3.2}$$

We have assumed that a PBNJ effectively increases the noise power level of the AWGN channel over which signal is transmitted. It is also assumed that the received waveform during a given hopping period is either jammed or jam-free. Therefore what we have to

estimate is E_s/N_t, the symbol signal energy to total noise power spectral density ratio in each hopping block.

We first notice that the DPSK demodulator output is given by

$$\begin{aligned} u_i &= r_i r_{i-1}^* = E_s x_i + \sqrt{E_s}(n_i + n_{i-1}^*) + n_i n_{i-1}^* \\ &= E_s x_i + w_i \end{aligned} \tag{3.3}$$

where $x_i \in \{+1, -1\}$. Here we have invoked the assumption of [12] that the combination of three noise terms is an equivalent Gaussian random variable $w_i \sim N(\mu_w, \sigma_w^2)$. Such an approximation simplifies the decoding metric computation at the cost of negligible performance degradation. Since the first and the second moments of this Gaussian random variable are given by

$$\begin{aligned} E\{w_i\} = \mu_w &= E\{\sqrt{E_s}(n_i + n_{i-1}^*) + n_i n_{i-1}^*\} \\ &= E\{\sqrt{E_s} n_i\} + E\{\sqrt{E_s} n_{i-1}^*\} + E\{n_i\}E\{n_{i-1}^*\} = 0 \qquad (3.4) \\ var\{w_i\} = \sigma_w^2 &= var\{\sqrt{E_s}(n_i + n_{i-1}^*) + n_i n_{i-1}^*\} \\ &= var\{\sqrt{E_s} n_i\} + var\{\sqrt{E_s} n_{i-1}^*\} + var\{n_i\}var\{n_{i-1}^*\} \\ &= E_s N_0 + \frac{N_0^2}{4} \qquad (3.5) \\ &\triangleq \frac{W_0^2}{2} \qquad (3.6) \end{aligned}$$

the probability of u_i conditioned on x_i becomes

$$p(u_i | x_i = \pm 1) = \frac{1}{\sqrt{\pi W_0^2}} \exp\left[-\frac{E_s^2}{W_0^2}(u_i \pm 1)^2\right] \tag{3.7}$$

and then

$$\begin{aligned} L\left(b_i | u_i\right) &= \ln \frac{p(u_i | b_i = 0) \cdot P(b_i = 0)}{p(u_i | b_i = 1) \cdot P(b_i = 1)} \\ &= \ln \frac{\exp\left[-\frac{E_s^2}{W_0^2}(u_i - 1)^2\right]}{\exp\left(-\frac{E_s^2}{W_0^2}(u_i + 1)^2\right)} + \ln \frac{P(b_i = 0)}{P(b_i = 1)} \\ &= 4 \cdot \frac{E_s^2}{W_0^2} \cdot u_i + L(b_i) \\ &= L_c \cdot u_i + L(b_i) \end{aligned} \tag{3.8}$$

Unlike the BPSK case, the required channel side information (CSI) for DPSK is E_s^2/W_0^2.

3.2 Performance loss due to SNR mismatch

Summers and Wilson [11] studied the sensitivity to SNR mismatch for turbo coded BPSK systems in an AWGN channel. They found that turbo coded systems are relatively robust to SNR mismatch. At low SNRs the decoder performance degradation is negligible as long as the SNR estimation error is between +1 dB and -2 dB. If SNR is high one can have an even larger estimation error tolerance (between +6 dB and -2 dB).

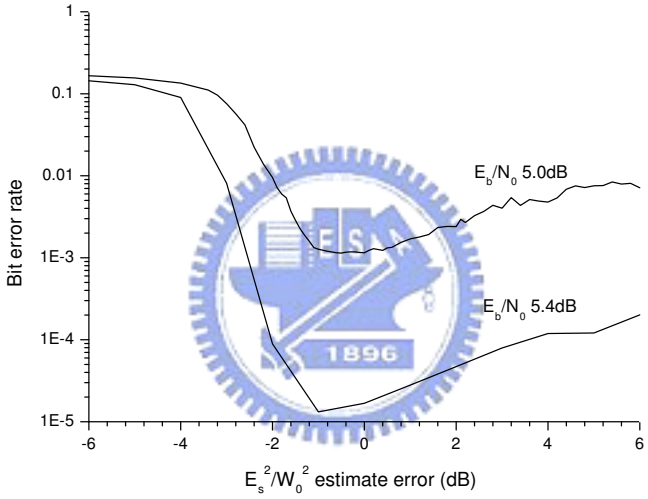

Figure 3.1: SNR sensitivity of a turbo coded DPSK system; code rate 1/3, interleaver size 400, {15,13} component codes, 10 decoding iterations; AWGN channel.

As we are more interested in DPSK waveform, we would like know the SNR sensitivities of turbo coded DPSK and IBPTC-coded DPSK systems. IBPTC is a turbo code that uses an IBP interleaver which performs intra-block interleaving and an extra inter-block interleaving. Fig. 3.1 and Fig. 3.2 depict the BER performance as a function of SNR estimation error. IBP turbo coded DPSK systems are more sensitive to SNR mismatch than its conventional turbo coded counterpart. As SNR estimation error

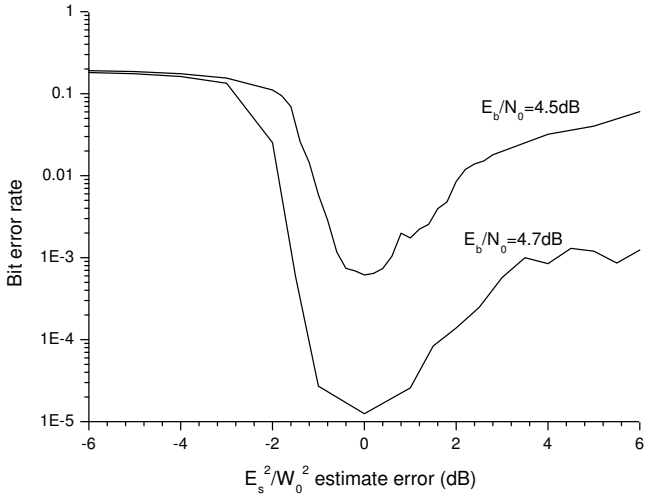

Figure 3.2: SNR sensitivity of a IBP-turbo coded DPSK system; code rate 1/3, interleaver size 400, {15,13} component codes, 10 decoding iterations; AWGN channel.

results in significant BER performance degradation in IBPTC-coded DPSK systems, it is important for an IBPTC decoder to have a reliable SNR estimator.

3.3 SNR estimation schemes

Several SNR estimators are presented in this section. Some are obtained using the so-called moment methods while others operate in a decision feedback manner, assuming perfect decisions.

3.3.1 Estimator A

In [11], an online SNR estimation method based on moments and second ordered polynomial curve fitting is proposed. For a BPSK system, the received matched filter output r_i has the following statistical properties:

$$E\{r_i^2\} = E_s + \sigma_{n^2} \tag{3.9}$$

$$E\{|r_i|\} = \sigma_n \sqrt{\frac{2}{\pi}} e^{-(E_s/2\sigma_n^2)} + \sqrt{E_s}\left[\text{erf}\left(\sqrt{\frac{E_s}{2\sigma_n^2}}\right)\right] \tag{3.10}$$

where $\mathrm{erf}(x)$ is the error function. Then the new variable z

$$z = \frac{E\{r_i^2\}}{[E\{|r_i|\}]^2} = \frac{1+\frac{E_s}{\sigma_{n^2}}}{\left\{\sqrt{\frac{2}{\pi}}e^{-(E_s/2\sigma_n^2)} + \sqrt{\frac{E_s}{\sigma_n^2}}\left[\mathrm{erf}\left(\sqrt{\frac{E_s}{2\sigma_n^2}}\right)\right]\right\}^2} = f\left(\frac{E_s}{\sigma_n^2}\right) \tag{3.11}$$

is a function of E_s/σ_n^2. Estimating the moments and z by time-averaging and curve fitting the inverse function $f^{-1}(\cdot)$, we then obtain the estimate $\widehat{\frac{E_s}{\sigma_n^2}} = f^{-1}(\hat{z})$.

This approach does not have a closed form expression for the inverse function and it is not suitable for a DPSK system needs an estimate of $\frac{E_s^2}{W_0^2}$ in stead. We present three SNR estimators that are also based on the moment method but do not need the nonlinear curve fitting coefficients.

Using the approximation

$$\mathrm{erf}\left(\sqrt{\frac{E_s}{2\sigma_n^2}}\right) \leq 1 - \frac{1}{\sqrt{\pi\frac{E_s}{2\sigma_n^2}}}, \quad E_s/2\sigma_n^2 \gg 1 \tag{3.12}$$

we obtain an SNR estimate for BPSK signals

$$z = \frac{E\{r_i^2\}}{[E\{|r_i|\}]^2} = \frac{1+\frac{E_s}{\sigma_n^2}}{\frac{E_s}{\sigma_n^2}} = 1 + \left(\frac{E_s}{\sigma_n^2}\right)^{-1} \tag{3.13}$$

$$\Rightarrow \frac{E_s}{\sigma_n^2} = \frac{1}{z-1}, \quad \frac{E_s}{N_0} = \frac{1}{2(z-1)} \tag{3.14}$$

For DPSK modulation, we have

$$z = \frac{E\{u_i^2\}}{(E\{|u_i|\})^2} = \frac{1+E_s^2/\sigma_w^2}{E_s^2/\sigma_w^2}$$

from which we obtain the MM-based SNR estimator of the first kind

$$E_s^2/\sigma_w^2 = \frac{1}{z-1} \quad \text{or, equivalently} \quad \frac{\widehat{E_s^2}}{W_0^2} = \frac{1}{2(z-1)} \tag{3.15}$$

For convenience, we refer to the above SNR estimator as Estimator A. Fig. 3.3 shows the performance of the mean and standard deviation performance of this estimator for three different SNRs. This estimator results in a positive bias due to the approximation

(3.11). Figs. 3.4 and 3.5 shows simulated BER performance when the receiver uses Estimator A and when perfect SNR is available. The code rate is 1/3, interleaver size is 400 and the decoder performs ten decoding iterations. The simulation results indicate that the performance loss due to imperfect SNR estimation is less than 0.1 dB for BER $= 10^{-5}$.

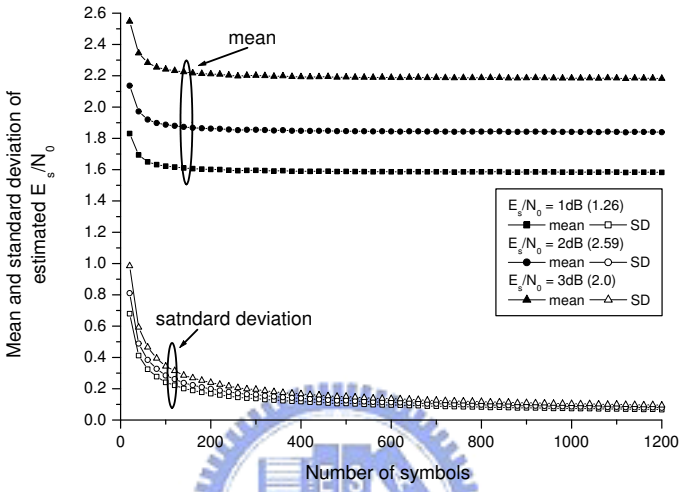

Figure 3.3: Mean and standard deviation performance of Estimator A.

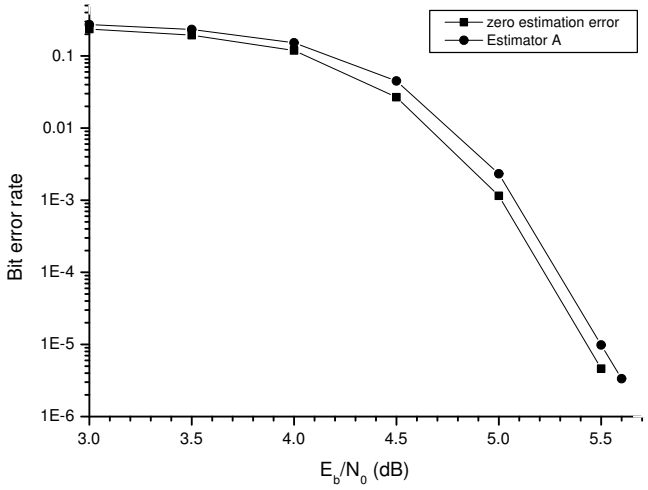

Figure 3.4: BER performance of a turbo coded DPSK system using perfect SNR and Estimator A with interleaver size 400 AWGN channel.

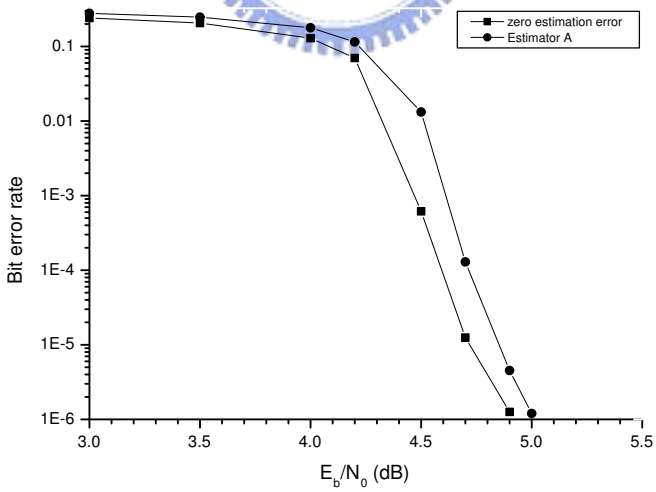

Figure 3.5: BER performance of an IBPTC-DPSK system using perfect SNR and Estimator A with interleaver size 400, AWGN channel.

3.3.2 Estimator B

Estimator A is a biased estimator with the bias depends on the true SNR. When SNR is low the bias becomes relatively large while the bias is negligible if SNR is high. We now present an SNR estimator which is almost unbiased no matter what the true SNR is.

For a coherent BPSK detector, the first four moments of its matched filter output are

$$E\{n_i\} = E\{n_i^3\} = 0, \quad E\{n_i^2\} = \sigma_n^2, \quad E\{n_i^4\} = 3\sigma_n^4$$

These moments imply

$$E\{r_i^2\} = E\{E_s + 2\sqrt{E_s}x_i n_i + n_i^2\} = E_s + \sigma_n^2 \tag{3.16}$$

$$\begin{aligned} E\{r_i^4\} &= E\{E_s^2 + 4(\sqrt{E_s})^3 x_i n_i + 6E_s n_i^2 + 4\sqrt{E_s}x_i n_i^3 + n_i^4\} \\ &= E_s^2 + 6E_s\sigma_n^2 + 3\sigma_n^4 \end{aligned} \tag{3.17}$$

and the relationships

$$3\left(E\{r_i^2\}\right)^2 - E\{r_i^4\} = 2E_s^2$$

$$E_s = \sqrt{\frac{3\left(E\{r_i^2\}\right)^2 - E\{r_i^4\}}{2}} \tag{3.18}$$

$$\sigma_n^2 = N_0/2 = E\{r_i^2\} - \sqrt{\frac{3\left(E\{r_i^2\}\right)^2 - E\{r_i^4\}}{2}} \tag{3.19}$$

which lead to Estimator B

$$\frac{\widehat{E_s}}{N_0} = \frac{\sqrt{\frac{3[E(r_i^2)]^2 - E(r_i^4)}{2}}}{2\left[E(r_i^2) - \sqrt{\frac{3[E(r_i^2)]^2 - E(r_i^4)}{2}}\right]} \tag{3.20}$$

where the expectations are replaced by time-averages.

Fig. 3.6 depicts the performance of Estimator B. It is obvious that the bias of this estimator is negligible regardless of the true SNR value as long as the number of symbols used for estimating is large enough, say > 300. Unfortunately, Estimator B does not work for DPSK systems.

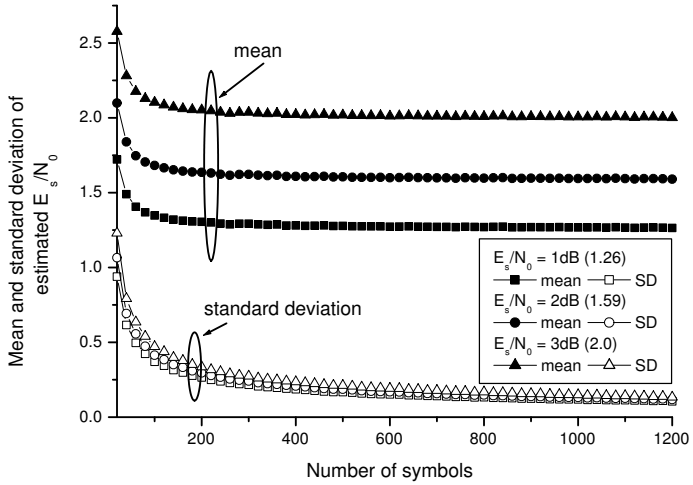

Figure 3.6: Mean and the standard deviation of Estimator B for coherent BPSK.

3.3.3 Estimator C

Consider the output of a DPSK demodulator.

$$u_i = r_i r_{i-1}^* = E_s x_i + \sqrt{E_s}(n_i + n_{i-1}^*) + n_i n_{i-1}^* \tag{3.21}$$

One can establish that

$$E\left(u_i^2\right) = E_s^2 + 2E_s\sigma_n^2 + \sigma_n^4 \tag{3.22}$$

$$E\left(u_i^4\right) = E_s^4 + 12E_s^3\sigma_n^2 + 18E_s^2\sigma_n^4 + 36E_s\sigma_n^6 + 9\sigma_n^8 \tag{3.23}$$

Since

$$W_0^2 = 2\sigma_w^2 = 2(2E_s\sigma_n^2 + \sigma_n^4) = 2\left[E\left(u_i^2\right) - E_s^2\right] \tag{3.24}$$

and

$$\begin{aligned}\left(E_s^2 + 6E_s\sigma_n^2 + 3\sigma_n^4\right)^2 &= E_s^4 + 12E_s^3\sigma_n^2 + 42E_s^2\sigma_n^3 + 36E_s\sigma_n^6 + 9\sigma_n^8 \\ &= E\left(u_i^4\right) + 24E_s^2\sigma_n^4 \qquad (3.25)\\ \Rightarrow E_s^2 + 6E_s\sigma_n^2 + 3\sigma_n^4 &= \sqrt{E\left(u_i^4\right) + 24E_s^2\sigma_n^4} \qquad (3.26)\end{aligned}$$

we obtain

$$\begin{aligned} E_s^2 &= \frac{3E\left(u_i^2\right) - \left(E_s^2 + 6E_s\sigma_n^2 + 3\sigma_n^4\right)}{2} \\ &= \frac{3}{2}E\left(u_i^2\right) - \sqrt{\frac{E\left(u_i^4\right)}{4} + 6E_s^2\sigma_n^4} \end{aligned} \tag{3.27}$$

Therefore,

$$\begin{aligned} \frac{E_s^2}{W_0^2} &= \frac{1.5E\left(u_i^2\right) - \sqrt{\frac{E\left(u_i^4\right)}{4} + 6E_s^2\sigma_n^4}}{2E\left(u_i^2\right) - 2\left[1.5E(u_i^2) - \sqrt{\frac{E(u_i^4)}{4} + 6E_s^2\sigma_n^4}\right]} \\ &= \frac{1.5E(u_i^2) - \sqrt{\frac{E(u_i^4)}{4} + 6E_s^2\sigma_n^4}}{-E(u_i^2) + 2\sqrt{\frac{E(u_i^4)}{4} + 6E_s^2\sigma_n^4}} \\ &= -1.5 + \frac{2\sqrt{\frac{E(u_i^4)}{4} + 6E_s^2\sigma_n^4}}{-E(u_i^2) + 2\sqrt{\frac{E(u_i^4)}{4} + 6E_s^2\sigma_n^4}} \\ &= -0.5 + \frac{E(u_i^2)}{-E(u_i^2) + 2\sqrt{\frac{E(u_i^4)}{4} + 6E_s^2\sigma_n^4}} \\ &= -0.5 + \frac{1}{-1 + 2\sqrt{\frac{E\left(u_i^4\right)}{4[E\left(u_i^2\right)]^2} + 6\left[\frac{E_s\sigma_n^2}{E\left(u_i^2\right)}\right]^2}} \end{aligned} \tag{3.28}$$

For $E_s/\sigma_n^2 \gg 1$

$$\left[\frac{E_s\sigma_n^2}{E\left(u_i^2\right)}\right]^2 = \left(\frac{E_s\sigma_n^2}{E_s^2 + 2E_s\sigma_n^2 + \sigma_n^4}\right)^2 = \left[\frac{1}{\left(\frac{E_s}{\sigma_n^2}\right) + 2 + \left(\frac{E_s}{\sigma_n^2}\right)^{-1}}\right]^2 \approx 0 \tag{3.29}$$

When $\left[\left(\frac{E_s}{\sigma_n^2}\right) + 2 + \left(\frac{E_s}{\sigma_n^2}\right)^{-1}\right]^2 \gg 1$, we obtain Estimator C

$$\widehat{\frac{E_s^2}{W_0^2}} = -1/2 + \frac{1}{-1 + 2\sqrt{\frac{E\left(u_i^4\right)}{4[E\left(u_i^2\right)]^2}}} = \frac{1}{\frac{\sqrt{E\left(u_i^4\right)}}{E\left(u_i^2\right)} - 1} - \frac{1}{2} \tag{3.30}$$

where the expectations are to be replaced by time averages. The resulting performance of this estimator is presented in Fig. 3.7. These performance curves demonstrate that it is an almost-unbiased estimator.

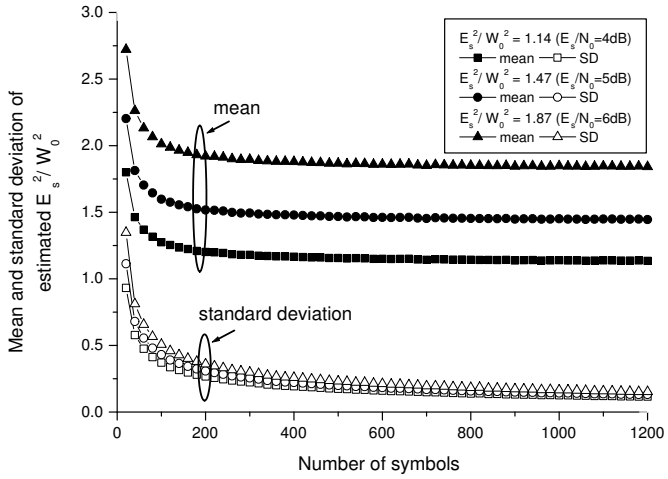

Figure 3.7: Mean and the standard deviation performance of Estimator C for DPSK modulation.

3.3.4 Decision-aided SNR estimator

An alternate candidate estimator is to use decisions for SNR estimation. Note that decisions are made based on the detector output u_i.

$$\begin{cases} \hat{x}_i = 1 & \text{if } \Re\{u_i\} \geq 0 \\ \hat{x}_i = -1 & \text{if } \Re\{u_i\} < 0 \end{cases} \tag{3.31}$$

Using the approximation $\hat{x}_i = x_i$ and the i.i.d. assumption of n_i in the product

$$\Re\{u_i\}\hat{x}_i = \Re\{r_i r_{i-1}^*\}\hat{x}_i = E_s x_i \hat{x}_i + \sqrt{E_s}\Re\{n_i + n_{i-1}^*\}\hat{x}_i + \Re\{n_i n_{i-1}^*\}\hat{x}_i \tag{3.32}$$

we obtain the estimate

$$\frac{\sum_{i=1}^{N_e} \Re\{u_i\}\hat{x}_i}{N_e} \approx E_s = \hat{E}_s \tag{3.33}$$

where N_e is the number of samples used in the estimate.

To estimate N_0, we use the relation

$$var\{u_i\} = E_s^2 + E_s\left(\frac{N_0}{2} + \frac{N_0}{2}\right) + \left(\frac{N_0}{2}\right)^2 = \left(E_s + \frac{N_0}{2}\right)^2 \tag{3.34}$$

which leads to

$$\hat{N}_0 = \sqrt{var\{u_i\}} - \hat{E}_s \tag{3.35}$$

$$\frac{\widehat{E_s}}{N_0} = \frac{\widehat{E}_s}{\widehat{N}_0} \tag{3.36}$$

Fig. 3.8 shows the mean and standard deviation of the above decision-aided estimator, which we refer to as Estimator D. Figs. 3.9 and 3.10 compare the mean and standard deviation performance of two biased estimators– Estimator A and Estimator D.

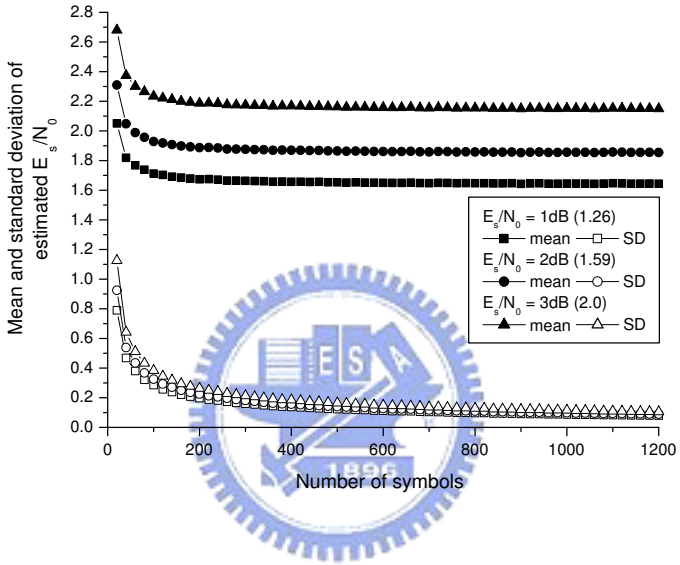

Figure 3.8: Mean and SD performance of decision-aided SNR estimator (Estimator D).

We find that the mean of Estimator A is closer to the exact value than Estimator D when $E_s/N_0 = E_b/(3N_0)$ is less than 1.59. The standard deviation performance of Estimator A is also smaller than that of Estimator D. For the turbo coded system under consideration, the SNR region we are interested in is $E_b/N_0 < 6$ dB. Since the code rate $R = 1/3$, the E_s/N_0 region of interest is less than 1.3 dB. Estimator A seems to be a better candidate in this region. However, this conclusion is based on the uncoded assumption, i.e., the decision is made right at the detector output which tends to give a high BER at low SNRs. If one uses the decoder decision which has much lower error rate, the performance of Estimator D would be much improved.

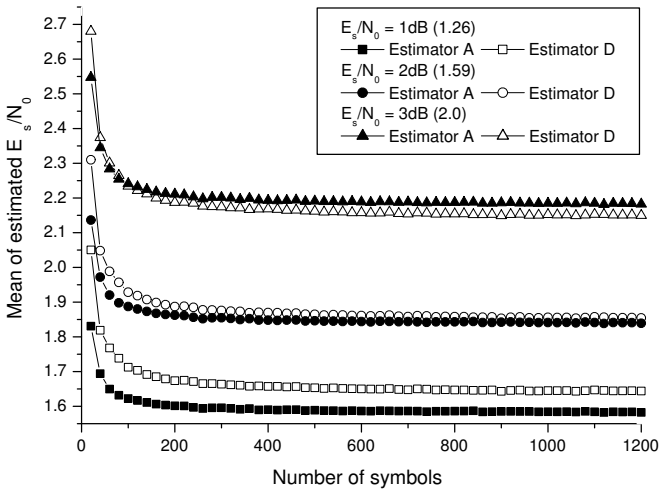

Figure 3.9: Mean of Estimator A and Estimator D.

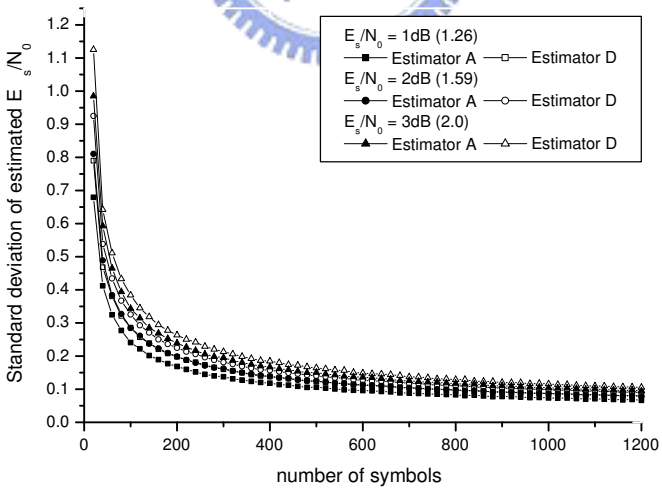

Figure 3.10: Standard deviation performance of the decision-aided estimator and Estimator A.

3.4 SNR estimator based on multiple hops

Numerical results presented in the above section indicate that Estimator C is the best choice for incoherent DPSK systems while Estimator B is best SNR estimate for coherent DPSK systems in terms of bias. In the subsequent discourse we will use these two estimators for incoherent and coherent DPSK systems, respectively.

Figs. 3.6 and 3.7 tell us that the performance of a SNR estimator improves as the number of symbols used increases. On the other hand, the AJ capability improves as the hopping rate increases or equivalently, as the number of bits per hop decreases. A higher hopping rate forces the jammer to distribute its total power over a wider bandwidth; see Fig. 2.3. But if the the number of bits per hop decreases the number of bits so is the number of samples used for estimating SNR. To solve this dilemma we propose the multiple-hop SNR estimation scheme shown in Fig. 3.11.

As bits in a hop are either jammed or unjammed, we need to determine whether a received block (hop) is jammed. Assuming the jamming strategy remain unchanged over a period of several hops, we associate each hop with either SNR_1 (jammed) and SNR_2 (jamming-free). Let C_1 and C_2 be the number of hops that belong to the jammed (SNR_1) and unjammed (SNR_2) categories, respectively. Every time a new block is received and the corresponding SNR estimate $\widehat{\mathrm{SNR}}$ is obtained, we classify this block according to the estimated SNR, checking whether it is closer to SNR_1 or SNR_2. Hence, after the SNR estimate $\widehat{\mathrm{SNR}}$ for the kth received hop is obtained, we update both representative SNR and the number of each class via

$$\hat{t} = \arg\min(|\widehat{\mathrm{SNR}} - \mathrm{SNR}_1|, |\widehat{\mathrm{SNR}} - \mathrm{SNR}_2|) \tag{3.37}$$

$$\mathrm{SNR}_{\hat{t}} = \left(\frac{C_{\hat{t}}}{C_{\hat{t}}+1}\right) \cdot \mathrm{SNR}_{\hat{t}} + \left(\frac{1}{C_{\hat{t}}+1}\right) \cdot \widehat{\mathrm{SNR}} \tag{3.38}$$

$$C_{\hat{t}} = C_{\hat{t}} + 1 \tag{3.39}$$

SNR_t is then used to normalize the received bit's reliability. However it is necessary to set an upper limit for the C_i because once the jammer change the jamming strategy, $\widehat{\mathrm{SNR}}$

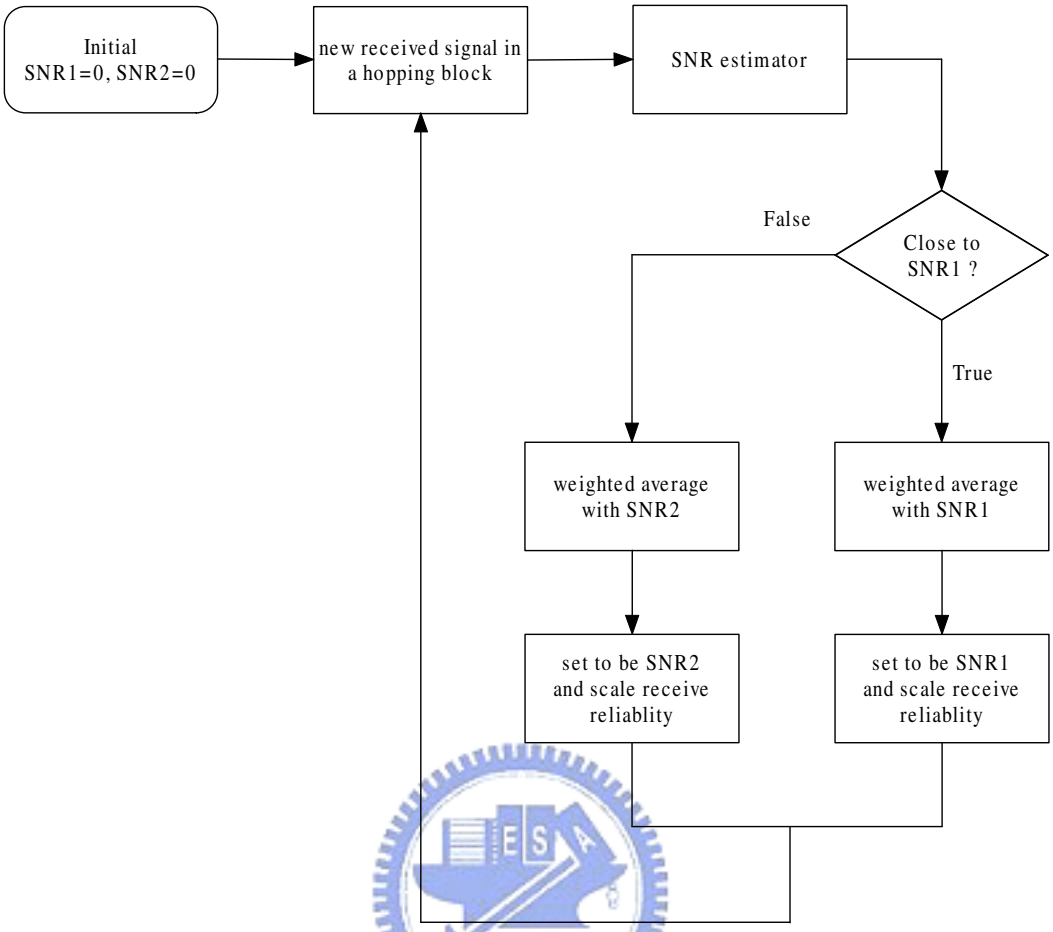

Figure 3.11: A multiple-hop SNR estimate scheme.

and SNR_t are likely to be far apart. By having an upper limit for C_i, the averaged SNR_t be able to track the true SNR closely. In our simulation we let the upper limit be 100 in this multiple-hop SNR estimator. One important assumption is that the jammer can change its jamming occupancy but the rate of the jammer changing jamming occupancy is very slow comparing to the speed that the averaged SNR_t adapt to the SNR of the new jamming occupancy.

Fig. 3.13 shows the simulation result of an IBP turbo coded FH/DPSK system with Estimator C. Since the hopping block size is 100, the number of symbols used to estimate SNR in every block is 100. It results in a performance degradation of 0.7 dB when compared with the perfect known SNR case shown in Fig. 3.12. For a full band

jammer an error floor around BER = 10^{-5} does exist. When the multiple-hop SNR estimate is used Fig. 3.14 shows that the performance degradation is reduced to 0.3dB and the performance in the presence of full band jammer, like that of a conventional turbo code, has a water-fall region around BER = 10^{-5}.

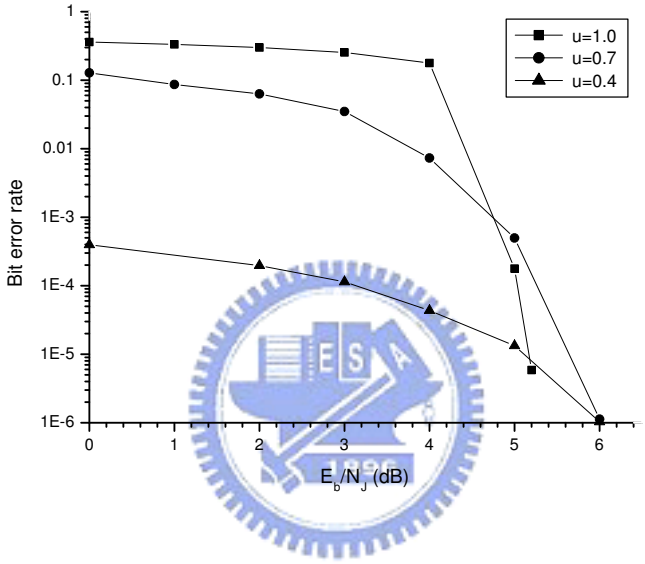

Figure 3.12: AJ performance of a turbo coded FH/DPSK system; interleaver size 400, perfect SNR estimate.

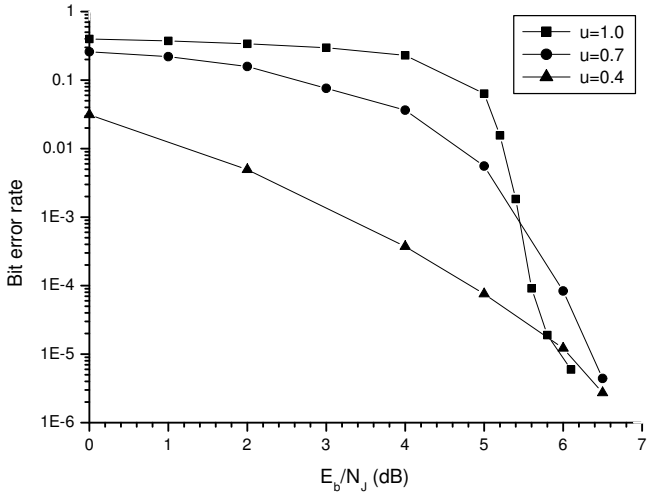

Figure 3.13: AJ performance of a turbo coded FH/DPSK system; interleaver size 400, Estimator C.

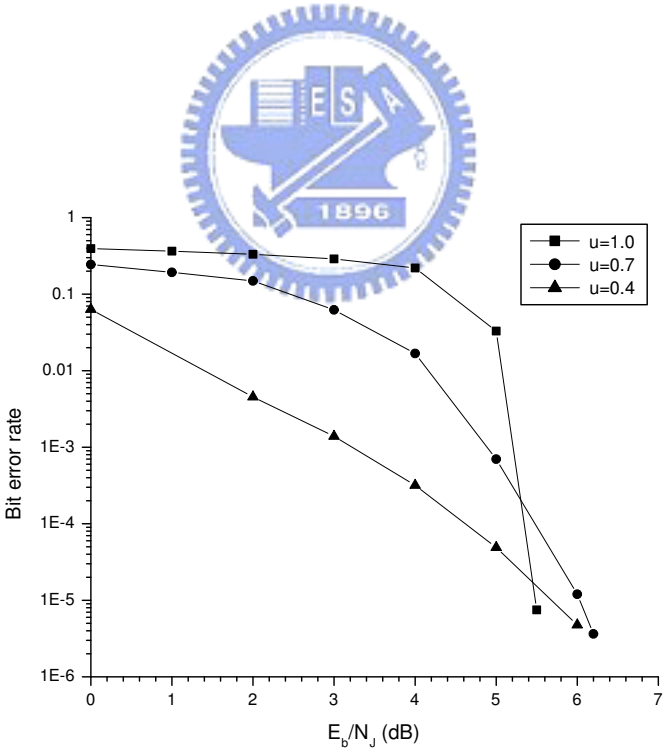

Figure 3.14: AJ performance of a turbo coded FH/DPSK system; interleaver size 400, multihop SNR Estimator C.

Chapter 4

IBP Turbo Codes and Decision-aided DPSK Detection

4.1 Turbo coded systems

A turbo code is composed of two parallel recursive systematic convolutional codes separated by an interleaver. It promises a BER performance close to the well known theoretical Shannon limit and was invented by Berrou *et al. Berrou* [2]. The key to the near Shannon-limit performance lies in the interleaver design and the iterative (turbo) decoding algorithm. Fig. 4.1 shows an exemplary turbo code defined by the 3GPP standard [7] while Fig. 4.2 presents a typical turbo decoder structure. For convenience of reference and comparison, we will use the corresponding convolutional codes and interleaver in our turbo coded systems. The input to the encoder is the data sequence $\{b_n : b_n = \pm 1\}$ and the output consists of three bit streams: the information bits $\{c_{0,i}\} = \{b_i\}$, the parity bit stream $\{c_{1,i}\}$ out of the first convolutional encoder and the parity bits $\{c_{2,i}\}$ out of the second convolutional encoder with the interleaved data stream $\{\pi(b_i)\}$ as the input. The soft-in soft-out decoder notated as $SISO_o$ is composed of two a posteriori probability (APP) decoders and an interleaver-deinterleaver pair. The APP decoders are responsible for computing the log-likelihood ratio and the so-called extrinsic information associated with each bit b_n based on the noise-corrupted versions of $\{c_{1,i}\}$ and $\{c_{2,i}\}$, respectively.

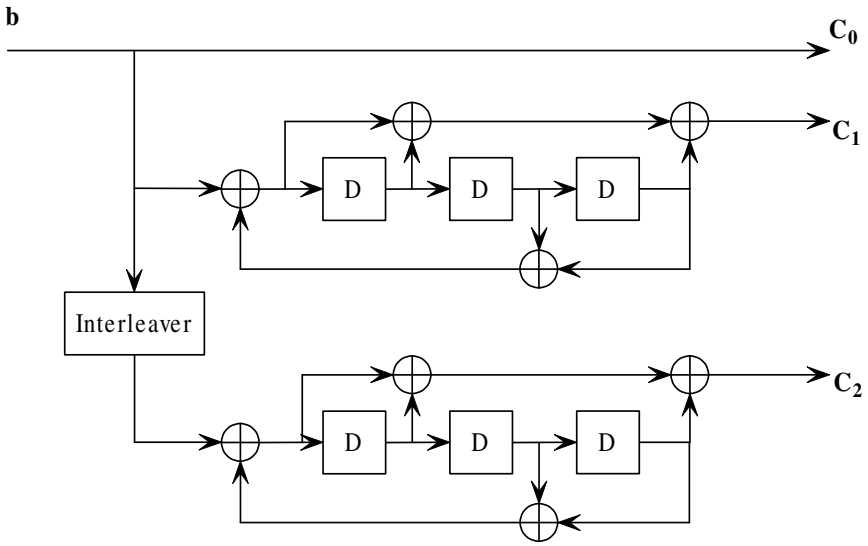

Figure 4.1: The turbo code encoder defined by the 3GPP standard.

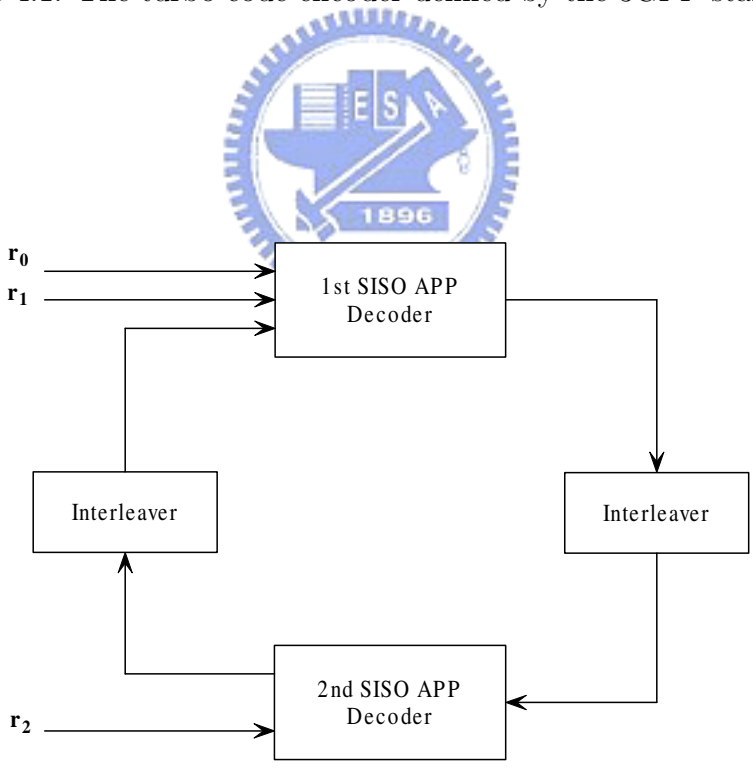

Figure 4.2: A turbo decoder structure (with zero internal delay).

The log-likelihood ratio of a given bit is a probabilistic reliability measure which is related to the corresponding a prior information and the extrinsic information. The first and the second APP decoders provides the reliability and extrinsic information about the data sequence $\{b_n\}$ and its interleaved version while the interleaver and the de-interleaver make sure that the extrinsic information is in right order. As shown in Fig. 4.2, the APP decoding process is carried out for several times until the decoder output meets some stopping criterion or a maximum number of iterations has been reached. For our turbo coded systems, the maximum number of decoding iteration is set to be 10 and no early-stopping mechanism is in place.

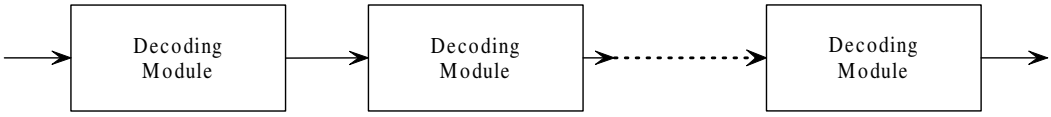

Figure 4.3: A modular pipelined turbo decoder.

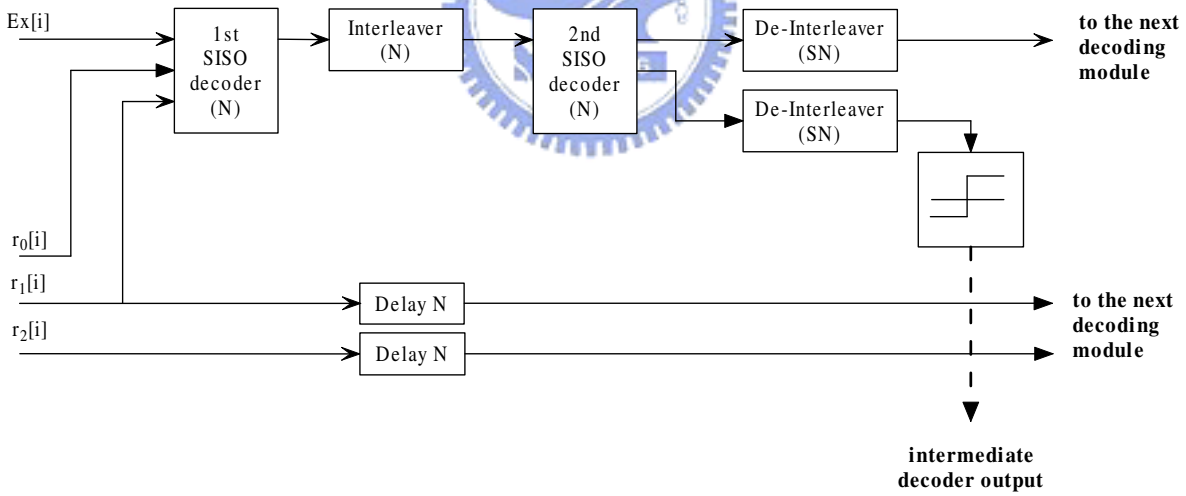

Figure 4.4: Decoding module for one decoding iteration.

The iteratively (turbo) decoding algorithm can be implemented as P pipelined identical elementary SISO decoders $SISO_{eo}$ [2]; see Figs. 4.3 and 4.4.

4.1.1 MAP decoding algorithm

The MAP decoding algorithm computes the conditional a posteriori probabilities of a bit given the observed sequence $\mathbf{r}$. It ensures the minimum symbol error probability performance. The corresponding log-likelihood ratio is given by

$$L_i(b_i) = \log \frac{P\{b_i = 1|\mathbf{r}_1^N\}}{P\{b_i = 0|\mathbf{r}_1^N\}} \tag{4.1}$$

where $1 \leq i \leq N_b$, N_b is the length of the information sequence and $\mathbf{r}_1^N$ is the vector representation of the received sequence of duration N samples. The decision about b_i is made based on

$$\begin{cases} 1 & L_i(b_i) \geq 0 \\ 0 & \text{otherwise} \end{cases} \tag{4.2}$$

Since

$$\begin{aligned} L_i(b_i) &= \log \frac{P\{b_i = 1|\mathbf{r}_1^N\}}{P\{b_i = 0|\mathbf{r}_1^N\}} \\ &= \log \frac{\sum_m \sum_{m'} P\{b_i = 1, S_i = m, S_{i+1} = m'|\mathbf{r}_1^N\}}{\sum_m \sum_{m'} P\{b_i = 0, S_i = m, S_{i+1} = m'|\mathbf{r}_1^N\}} \\ &= \log \frac{\sum_m \sum_{m'} P\{b_i = 1, S_i = m, S_{i-1} = m'\mathbf{r}_1^{i-1}, \mathbf{r}_i, \mathbf{r}_{i+1}^N\}}{\sum_m \sum_{m'} P\{b_i = 0, S_i = m, S_{i-1} = m'\mathbf{r}_1^{i-1}, \mathbf{r}_i, \mathbf{r}_{i+1}^N\}} \\ &= \log \frac{\sum_m \sum_{m'} P\{b_i = 1, S_i = m, \mathbf{r}_i, \mathbf{r}_{i+1}^N|S_{i-1} = m'\mathbf{r}_1^{i-1}\} \cdot P\{S_{i-1} = m', \mathbf{r}_1^{i-1}\}}{\sum_m \sum_{m'} P\{b_i = 0, S_i = m, \mathbf{r}_i, \mathbf{r}_{i+1}^N|S_{i-1} = m'\mathbf{r}_1^{i-1}\} \cdot P\{S_{i-1} = m', \mathbf{r}_1^{i-1}\}} \end{aligned}$$

$$= \log \frac{\sum_m \sum_{m'} P\{b_i = 1, S_i = m, \mathbf{r}_i, \mathbf{r}_{i+1}^N | S_{i-1} = m'\} \cdot \alpha_{i-1}(m')}{\sum_m \sum_{m'} P\{b_i = 0, S_i = m, \mathbf{r}_i, \mathbf{r}_{i+1}^N | S_{i-1} = m'\} \cdot \alpha_{i-1}(m')}$$

$$= \log \frac{\sum_m \sum_{m'} P\{b_i = 1, S_i = m, \mathbf{r}_i, \mathbf{r}_{i+1}^N, S_{i-1} = m'\} \cdot \alpha_{i-1}(m')}{\sum_m \sum_{m'} P\{b_i = 0, S_i = m, \mathbf{r}_i, \mathbf{r}_{i+1}^N, S_{i-1} = m'\} \cdot \alpha_{i-1}(m')}$$

$$= \log \frac{\sum_m \sum_{m'} P\{\mathbf{r}_{i+1}^N | b_i = 1, \mathbf{r}_i, S_i = m, S_{i-1} = m'\} \cdot \alpha_{i-1}(m')}{\sum_m \sum_{m'} P\{\mathbf{r}_{i+1}^N | b_i = 0, \mathbf{r}_i, S_i = m, S_{i-1} = m'\} \cdot \alpha_{i-1}(m')}$$

$$= \log \frac{\sum_m \sum_{m'} P\{\mathbf{r}_{i+1}^N | S_i = m\} \cdot P\{b_i = 1, \mathbf{r}_i, S_i = m, S_{i-1} = m'\} \cdot \alpha_{i-1}(m')}{\sum_m \sum_{m'} P\{\mathbf{r}_{i+1}^N | S_i = m\} \cdot P\{b_i = 0, \mathbf{r}_i, S_i = m, S_{i-1} = m'\} \cdot \alpha_{i-1}(m')}$$

$$= \log \frac{\sum_m \sum_{m'} \beta_i(m) \cdot P\{b_i = 1, \mathbf{r}_i, S_i = m, S_{i-1} = m'\} \cdot \alpha_{i-1}(m')}{\sum_m \sum_{m'} \beta_i(m) \cdot P\{b_i = 0, \mathbf{r}_i, S_i = m, S_{i-1} = m'\} \cdot \alpha_{i-1}(m')}$$

$$= \log \frac{\sum_m \sum_{m'} \alpha_{i-1}(m) \cdot P\{b_i = 1, \mathbf{r}_i, S_i = m | S_{i-1} = m'\} \cdot \beta_i(m)}{\sum_m \sum_{m'} \alpha_{i-1}(m) \cdot P\{b_i = 0, \mathbf{r}_i, S_i = m | S_{i-1} = m'\} \cdot \beta_i(m)}$$

We have the BCJR form of the log-likelihood ratio

$$L_i(b_i) = \log \frac{\sum_m \sum_{m'} \alpha_{i-1}(m') \cdot \gamma_i^1(m, m') \cdot \beta_i(m)}{\sum_m \sum_{m'} \alpha_{i-1}(m') \cdot \gamma_i^0(m, m') \cdot \beta_i(m)} \tag{4.3}$$

where the auxiliary parameters are defined by

$$\alpha_i(m) = P\{S_i = m, \mathbf{r}_1^i\} \tag{4.4}$$

$$\beta_i(m) = P\{\mathbf{r}_{1+1}^N | S_i = m\} \tag{4.5}$$

$$\gamma_i(m, m') = P\{S_i = m', \mathbf{r}_i | S_{i-1} = m\} \tag{4.6}$$

These parameters (decoding metrics) have probabilistic interpretations:

- $\alpha_i(m)$ is the forward state metric which can be seen as the probability of being at state m at time i given the observation of the received sequence from the beginning to time instant i.
- $\beta_i(m)$ is the backward state metric which is the probability of the received sequence form time instant $i+1$ to the end given that the encoder state is m at time instant i.

- $\gamma_i(m)(m')$ is the branch metric which is the probability of receiving $\mathbf{r}_i$ and being at state $S_i = m'$ given the previous state $S_{i-1} = m$.

Moreover, the forward and backward state metrics can be recursively computed via

$$\alpha_i(m') = \sum_{m=0}^{M-1} \alpha_{i-1}(m) \cdot \gamma_i(m, m') \tag{4.7}$$

$$\beta_i(m) = \sum_{m'=0}^{M-1} \beta_{i+1}(m') \cdot \gamma_i(m, m'). \tag{4.8}$$

Proper boundary conditions for $\alpha_i(0)$ and $\beta_i(N)$ should be given, depending on how $\{b_n\}$ and $\{\pi(b_n)\}$ are encoded. In case of RSC encoders, the received values $\mathbf{r}_i$ are split into two component vectors, representing the systematic and parity parts.

$$\mathbf{r}_i = (y_i^s, y_i^p) \tag{4.9}$$

and the branch metric can be separated into the following two terms according to whether 1 or 0 is transmitted.

$$\gamma_i^1 = p(y_i^s|b_i = 1) \cdot p(y_i^p|b_i = 1, S_i = m, S_{i-1} = m') \cdot \pi(S_i = m|S_{i-1} = m') \tag{4.10}$$

$$\gamma_i^0 = p(y_i^s|b_i = 0) \cdot p(y_i^p|b_i = 0, S_i = m, S_{i-1} = m') \cdot \pi(S_i = m|S_{i-1} = m') \tag{4.11}$$

where $\pi(S_i = m|S_{i-1} = m')$ is the state transition probability and is a function of the encoder structure and input statistic. For an AWGN channel,

$$\log\left[p(y_i^s|b_i = l)\right] = 2\frac{E_s}{N_0} x_i^s(l) y_i^s \tag{4.12}$$

$$\log\left[p(y_i^p|b_i = l)\right] = 2\frac{E_s}{N_0} x_i^p(l) y_i^p \tag{4.13}$$

where $x_i^s(l)$ and $x_i^p(l)$ are the systematic and parity bits when the ith information bit is $l(= 1 \text{ or } -1)$. E_s/N_0 has to estimated by a proper algorithm given in the last chapter.

4.2 Inter-block permutation (IBP)

Inter-block permutation (IBP) has been shown to be a effective interleaving rule in enhancing the performance of a turbo code regardless of what component codes are

used [8, 9]. IBP is actually a two-step permutation procedure that consists of an intra-block permutation and an intra-block permutation which further permutes the contents of intra-block permuted blocks. With an IBP interleaver, unbounded interleaving depth with bounded decoding delay is achievable and parallel real-time decoding is made easy. The BER performance curve of an inter-block permutation turbo code (IBPTC) usually has a very sharp waterfall and a low error floor even with a small latency constraint.

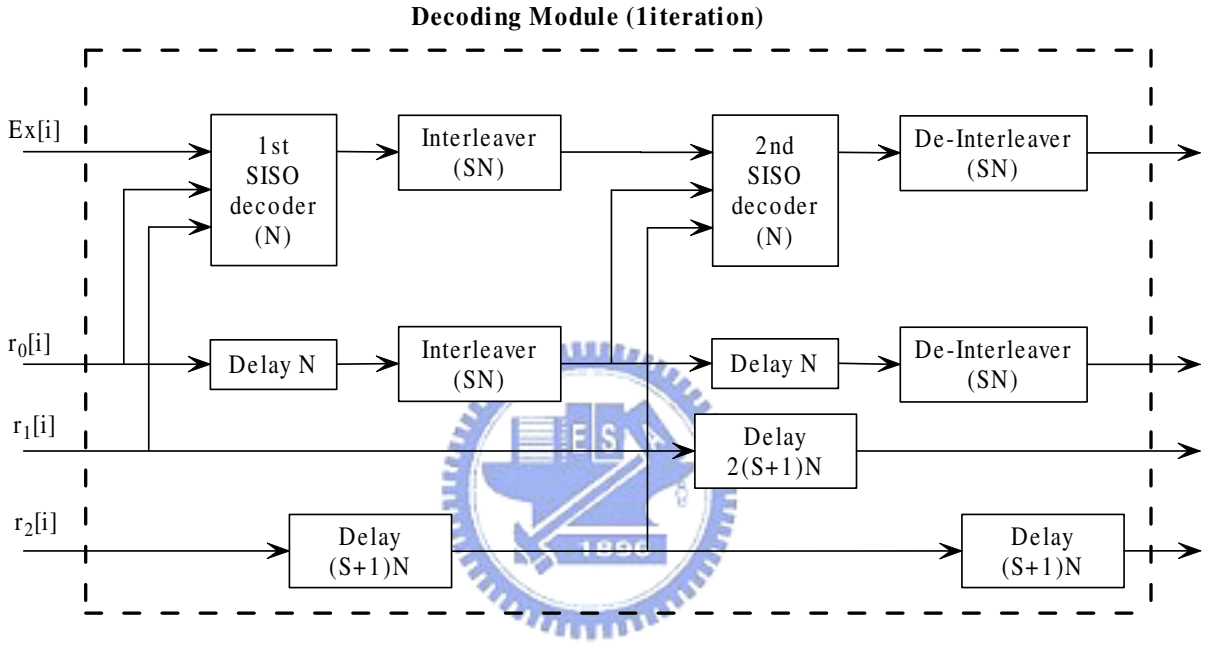

Figure 4.5: An IBP turbo decoder module.

Two IBP algorithms are proposed in [9] and we will use the one given in Table 4.1 as our inter-block permutation rule.

4.3 IIR filtered turbo DPSK structure

In the previous work, we have presented a turbo coded FH/DPSK system and introduced IBP turbo codes for AJ purpose. We expect the additional inter-block permutation performed amongst adjacent blocks within which more hops exist will force the jammer to distribute its power in larger band and reduce its jamming effectiveness.

Table 4.1: An IBP Algorithm [9].

```
Variables
I[S] - block index
N - interleaver block size
K - block number index
D(i,k) - data on the k-th block i-th position
Initialization
K=0
Recursion
for i=o to S-1
    if (K mod (2·(i+1)) < i+1)
        I[i]=0
    else
        I[i]=1
for i=0 to S-1
    m=I[i]+2·i+1
    for k=m k+=2S+1 k < N
        D(k,K)⟷D(k,K-i-1)
K++
```

On the other hand, it is known that a turbo coded incoherent DPSK system suffers a 3.5 dB performance degradation against a BPSK system [13]. This degradation can be minimized by applying methods such as multiple-symbol differential detection (MSDD), which detects a transmitted symbol based on the observation over a sequence of received symbols, or the differential detection with IIR filter (DDIIR) approach, which enhances the DPSK performance to the extent that the performance loss is almost negligible [6]. The latter approach will used in our system.

In the following subsections, we will discuss how to modify the DDIIR structure and apply it to our either turbo coded FH/DPSK or IBP turbo coded FH/DPSK systems.

4.3.1 Decision-aided DPSK differential detection

DPSK modulation is often used for terrestrial and satellite mobile communication systems because it does not a carrier recovery circuit and has fast acquisition performance. A DPSK demodulator recovers the information bit by comparing the phase

difference of two consecutive symbols. Since the decision involves samples from two symbol periods, more noise is introduced. Thus the energy per bit to noise power density ratio (E_b/N_0) required for DPSK incoherent detection is higher than that required for coherent DPSK detection to attain the same BER under the same channel condition. To improve the performance of a differential coherent DPSK receiver, several remedies have been proposed.

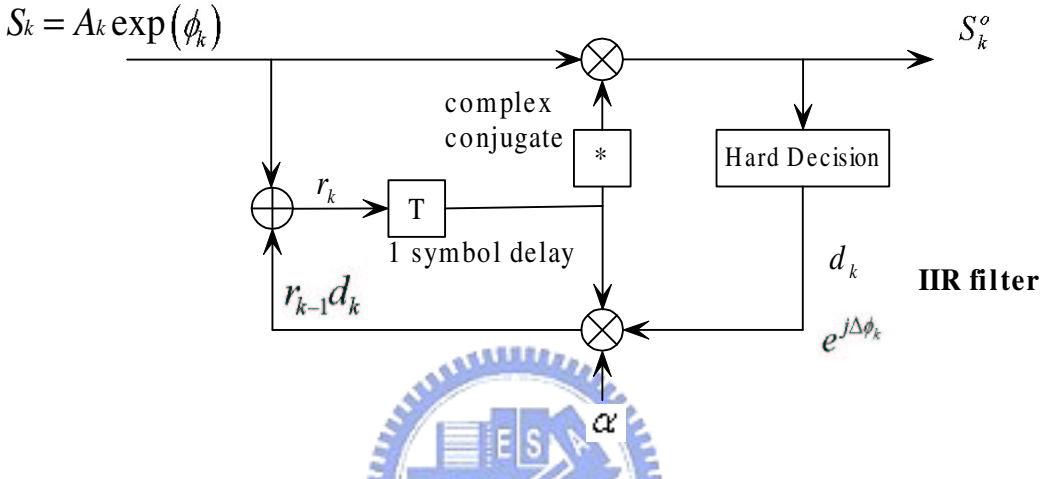

Figure 4.6: Block diagram of DDIIR scheme

Fig. 4.6 is the DDIIR structure proposed in [6]. This DDIIR scheme has a desirable characteristic that a wide range of performance between coherent and differential detection is achievable by simply changing the real valued weighting parameter α. When α is chosen to be close to 1 (see Fig. 4.6), the resulting BER performance becomes very close to that of differentially encoded coherently detected PSK (DEPSK) while if α is chosen to be 0, the performance is just that of an incoherent DPSK detector.

4.3.2 Phase compensated DDIIR

It had been showed that the DDIIR structure for increasing the reference bit SNR can improve DPSK detection performance [6]. With this detection structure, the BER performance in AWGN channels comes very close to that of a coherent DPSK detector. Since the detection BER performance is close to that of coherent detection, we can treat

the output of the hard decision signals as coherent DPSK decision output signals and further use them to estimate the phase offset ϕ_0. We will name the modified structure as the phase compensated DDIIR filter; see Fig. 4.7. The filter is basically composed of two parts, one is the DDIIR part whose responsibility is to increase the reference bit SNR and the other part is responsible for phase estimation and compensation.

In the second part, the decision $e^{j\triangle\phi_i}$ is sent to an accumulative multiplier whose output value is conjugated, giving $e^{-j\bar{\phi}_i}$. Phase offset estimation $\overline{\phi_0}$ is obtained by (i) multiplying the the received sample by $e^{-j\bar{\phi}_i}$ and (ii) averaging the accumulated product. The estimated phase offset will become more reliable as the accumulation time increases.

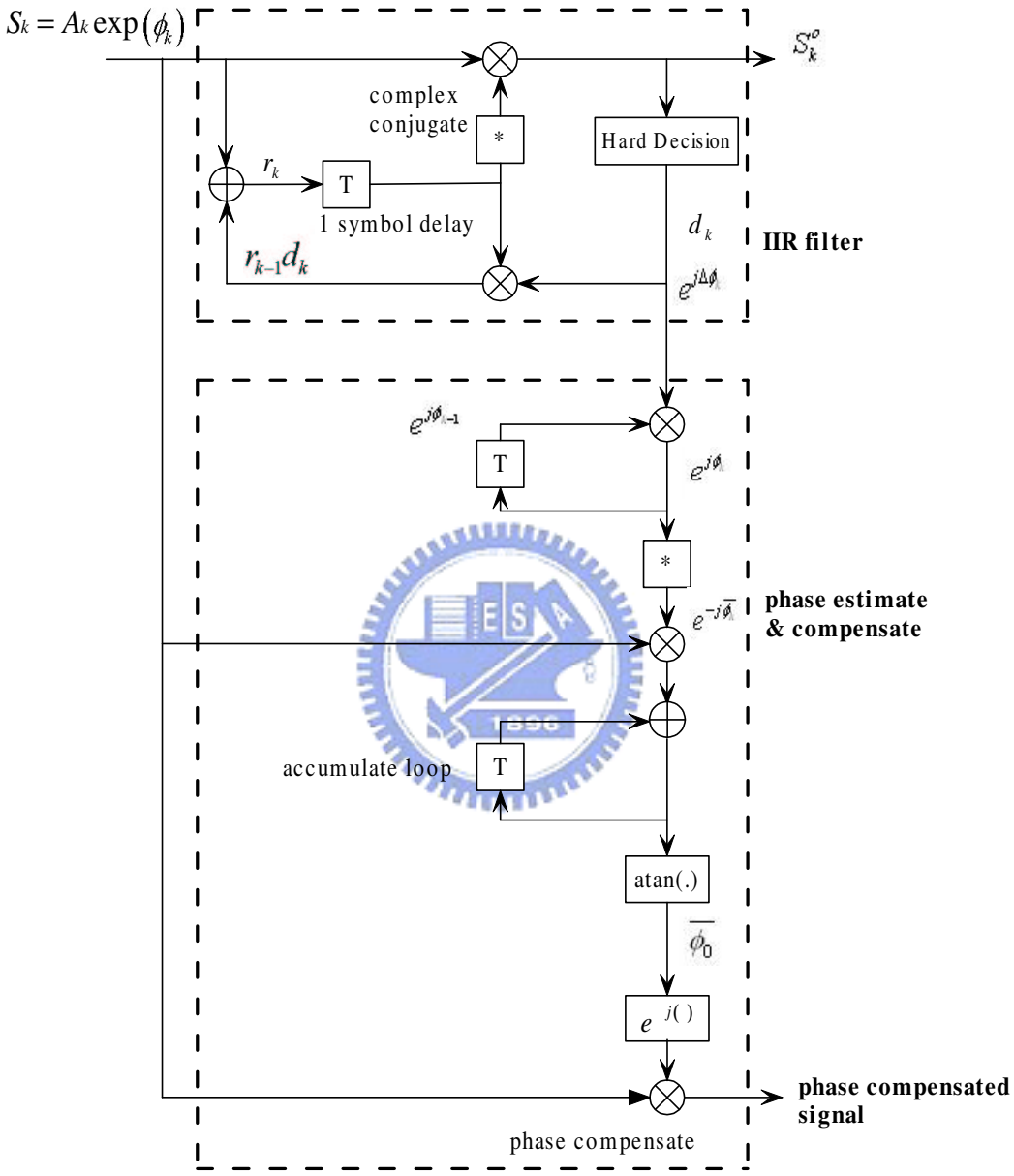

Figure 4.7: Structure of the phase compensated DDIIR filter.

4.3.3 Turbo DPSK receiver with phase estimation

Suppose the phase offset has been compensated for, we can compute the soft values of phase compensated channel information. The original DPSK demodulator can then be replaced with a soft in soft out (SISO) decoder, we denote the inner SISO decoder as $SISO_i$ and the outer SISO decoder as $SISO_o$. The receiver that iteratively decodes the serial concatenated coded waveform is henceforth called the *turbo DPSK* detector. The turbo coded DPSK system with the proposed receiver structure is referred to as the IIR-filtered turbo DPSK receiver as shown in Fig. 4.8.

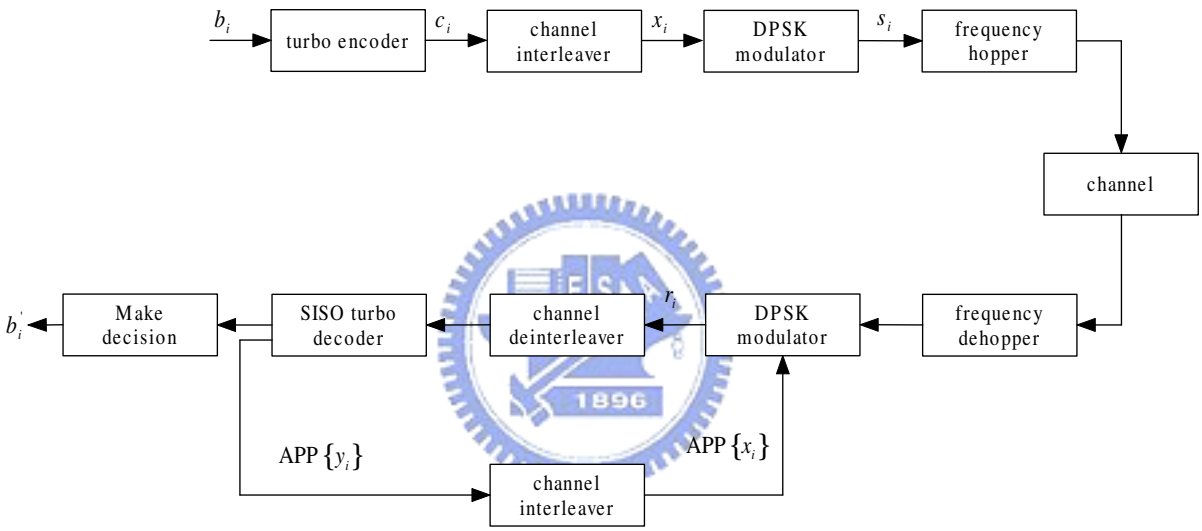

Figure 4.8: Block diagram of the IIR-filtered turbo DPSK system.

The iterative decoding procedure between inner DPSK SISO decoder and the outer turbo code decoder is summarized in the following.

1. Scale the real part values of the received phase compensated signal to provide channel information for the codeword bits of the inner code. For the first iteration, set the a priori probability equal-likely.

2. Calculate $\gamma_i(m, m')$, $\alpha_i(m')$, and $\beta_i(m)$ with the recursive computation equations we had talked in the previous section of MAP decoding algorithm. Then compute

the extrinsic information λ_j.

3. Deinterleave the stream of λ_j to λ_i as be the log-likelihood ratio (LLR) input for the code word bits of the outer code.

4. Run the turbo decoding procedure as mentioned before and compute the extrinsic information of the information bits.

5. Encode the extrinsic information of the information bits to get extrinsic information of the code word bits and interleave them to be a priori information for the next iteration inner decoding.

6. Go back to step.2 and begin the next decoding iteration. Or stop the procedure in step.5 and make decision if the maximum number of iterations is reached.

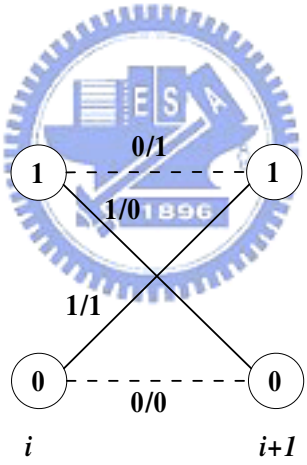

Figure 4.9: State diagram of differential encoder.

Note that because the inner encoder is a two-state differential encoder, Step 2 can be simplified without recursively computing the backward state metrics. Consider the state diagram of differential encoder in Fig. 4.9. When computing the backward state metric for each state in instant i, it has a metric path of bit 0 from the state 0 in instant $i+1$ and a metric path of bit 1 from the state 1 in instant $i+1$. Thus the backward state

metrics will all be equal after recursive computation. Therefore it has no contribution to the inner decoding.

We know that using an IIR filter to estimate the phase offset the estimated phase will be more accurate as the symbol index i increase. In other words, the phase compensation for the beginning symbols in each code word may not be good enough. Therefore we should have some special design for the IIR filtered turbo DPSK pipeline structure as Fig. 4.10. Since the turbo decoded systems have to implement in pipelined structure, the received signals should be delayed for the next decoding module. And the IIR filter estimated phase in the last last symbol index is always the most accurate one. We can use the estimated phase in the last last symbol index to do phase compensation of the pipeline delayed signals for the decoding iterations other than one. This action has to be done only once as illustrated in Fig. 4.10.

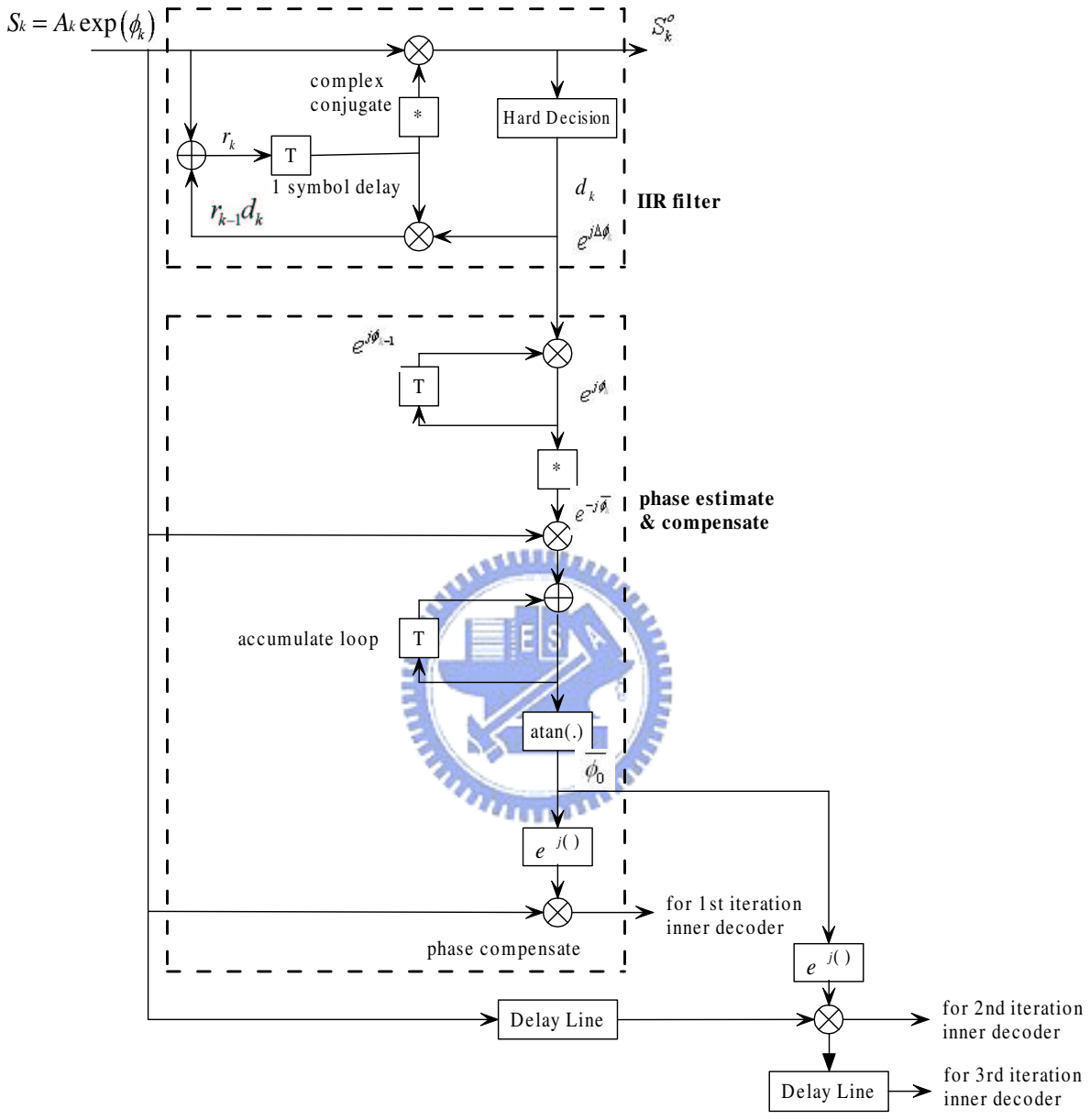

Figure 4.10: A pipeline IIR filtered turbo DPSK receiver structure.

Chapter 5

Uplink Performance: Numerical Results and Discussion

In this chapter we report the simulated performance of the four system structures we have presented, namely, turbo coded DPSK, IBPTC coded DPSK, IIR filtered turbo coded DPSK and IIR filtered IBPTC coded DPSK systems. The interleaver size is assumed to be 400. Furthermore, each system structure with different turbo encoder interleaver size are simulated in the communication environment of PBNJ interference with AWGN background noise. Error correcting ability of turbo codes can be enhanced by increasing the encoder interleaver size. We will see how large the interleaver size is enough for each receiver structure to force the PBNJ jammer distribute his jamming power over the full spreading spectrum. It means that we want the intersections of the full band jamming BER performance curve and the other jamming occupancy BER performance curve lie in very low BER, such as 10^{-5}. Then the four system structures with suitable turbo encoder interleaver size will be simulated more practically by introducing the nonlinearity effect of the TWTA subsystem.

5.1 Performances in AWGN channels

To begin with, we consider the case where the only channel perturbation is AWGN and no FH is employed. The system parameters for all receiver structures are identical: code rate = 1/3, interleaver size = 400 and {15,13} component codes are used. Our

simulation run stops whenever 50 (or 100) frame errors are detected.

From Figs. 5.1-5.3, we conclude that to reach a BER $= 10^{-5}$, the required E_b/N_0 for turbo coded, IBP turbo coded, IIR filtered turbo and IIR filtered IBPTC DPSK systems are 5.4 dB, 4.7 dB, 4.6 dB and 4.1 dB, respectively. It means that by using an IBPTC, 0.7 dB is gained. The IIR filtered mechanism provides a 0.8 dB gain to the turbo coded DPSK system and a 0.6 dB gain to the IBPTC coded DPSK system.

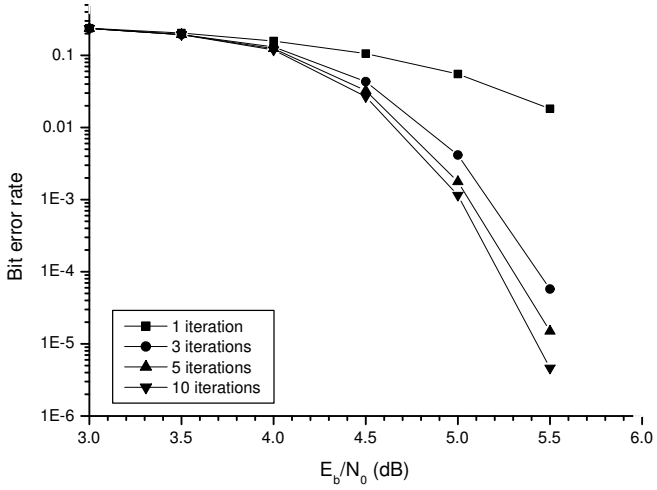

Figure 5.1: BER performance of a turbo coded DPSK system.

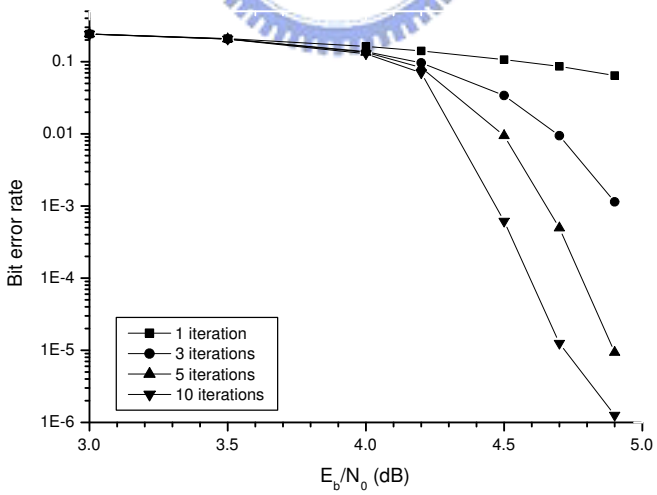

Figure 5.2: BER performance of an IBPTC coded DPSK system.

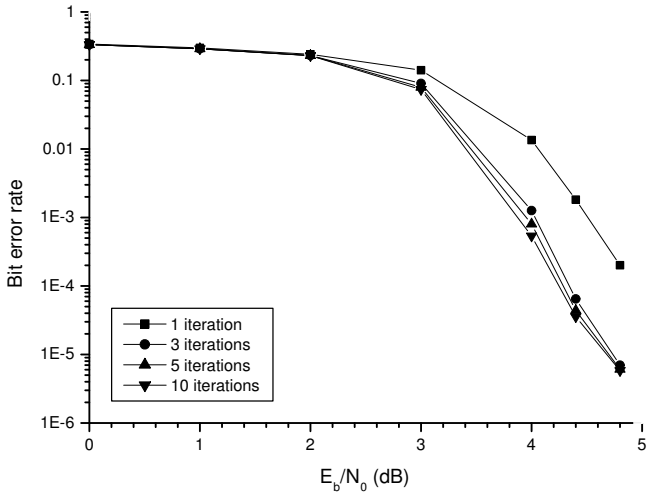

Figure 5.3: BER performance of an IIR filtered turbo coded DPSK system.

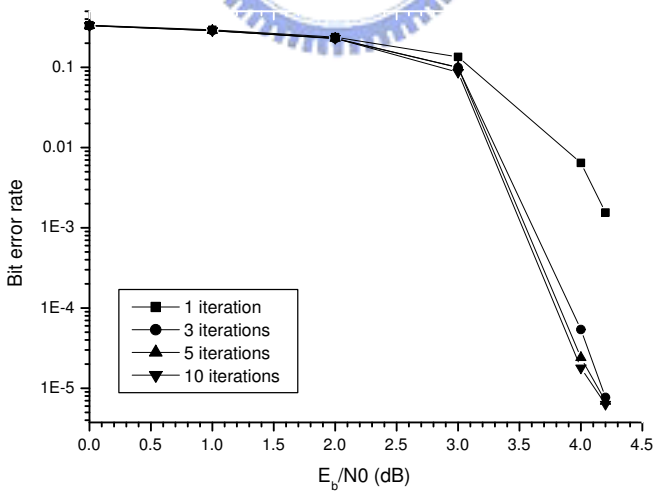

Figure 5.4: BER performance of an IIR filtered IBPTC DPSK system.

5.2 Performances in PBNJ interference and AWGN

Numerical results reported in this section assume the presence of PBNJ in addition to AWGN. All the system parameter values are the same as before except for the interleaver size. We consider interleaver with sizes 400, 800 ,1600 and 3200. It is known that the larger the size of interleaver is the more powerful the error correcting ability of the associated turbo code becomes and thus the more coding gain and better AJ capability we obtain. To have a fair comparison between IBP turbo coded and conventional turbo coded systems, the interleaver size of the latter should be twice as large as that of the former system since the IBP span is only 1.

Figs. 5.5-5.12 show the performance of various DPSK systems for different interleaving sizes. The optimal interleaving sizes for them are 3200, 3200, 1600 and 1600, respectively. The jammer will be forced to be jam the full band. The worst case for each system with a proper interleaver size is summarized in Table 5.1.

Table 5.1: System performance comparison (known $E_b/N_0 = 15$ dB but without nonlinearity effect).

system structure	proper interleaver size	SJR for BER 10^{-5}
turbo coded FH/DPSK	3200	5.1 dB
IIR filtered turbo coded FH/DPSK	3200	3.7 dB
IBP turbo coded FH/DPSK	800 (1600)	5 dB (4.8 dB)
IIR filtered IBP turbo coded FH/DPSK	1600	4.05 dB

We compare the AJ performance of the IBPTC coded FH/DPSK system using an interleaving size of 1600 with that of the turbo coded FH/DPSK system using an interleaving size of 3200, as both systems have the same encoding and average decoding delays. The IBPTC provides a 0.3 dB gain against conventional turbo coded system at BER = 10^{-5}. With the same delays, to have BER = 10^{-5} at SJR = 5 dB, the IBPTC system need an interleaver size of 800 while the conventional turbo coded system needs 3200–that is four-fold increase in the interleaver size and two-fold increase in decoding

delay.

5.2.1 Turbo coded FH/DPSK systems

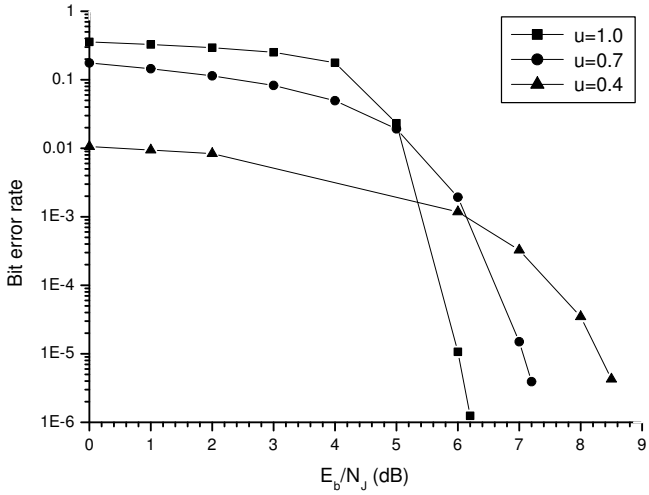

Figure 5.5: AJ performance of a turbo coded DPSK system; interleaver size 400, $E_b/N_0 =$ 15 dB.

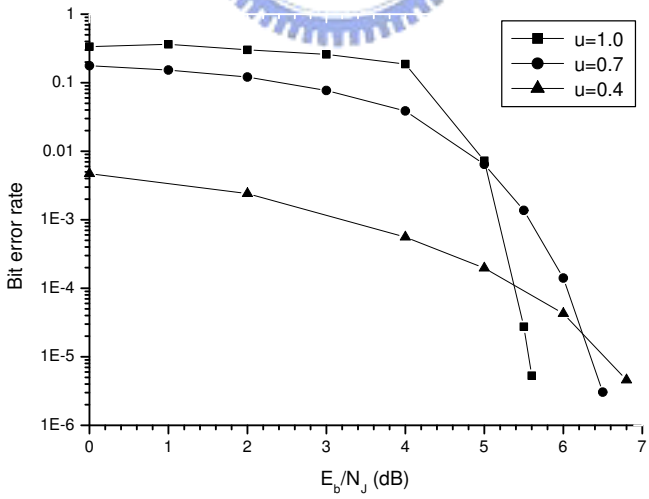

Figure 5.6: AJ performance of a turbo coded DPSK system; interleaver size 800, $E_b/N_0 =$ 15 dB.

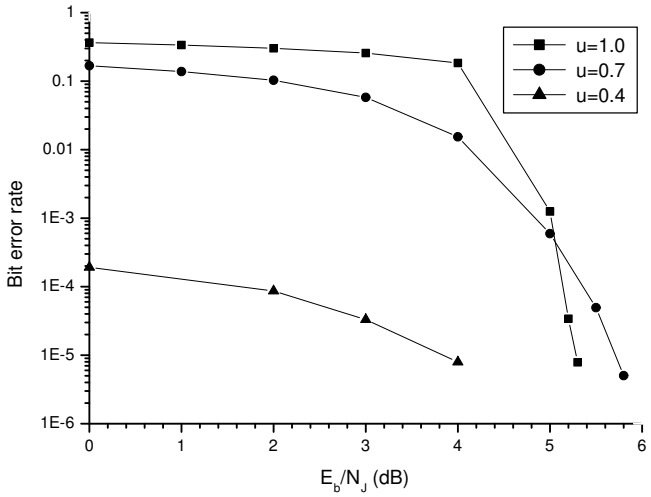

Figure 5.7: AJ performance of a turbo coded DPSK system; interleaver size 1600, $E_b/N_0 = 15$ dB.

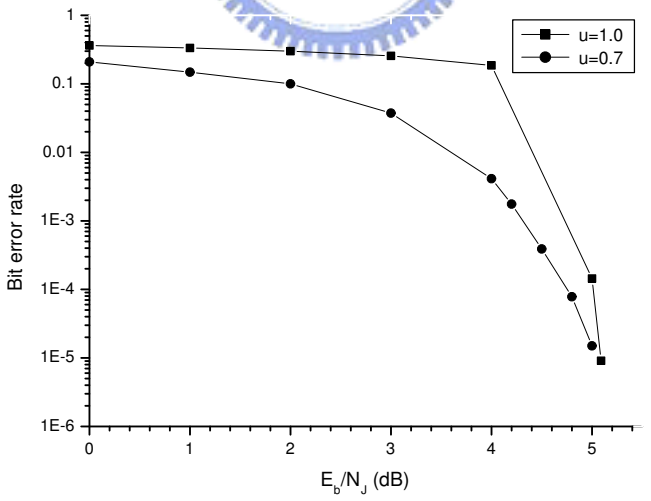

Figure 5.8: AJ performance of a turbo coded DPSK system; interleaver size 3200, $E_b/N_0 = 15$ dB.

5.2.2 IIR-filtered turbo coded FH/DPSK systems

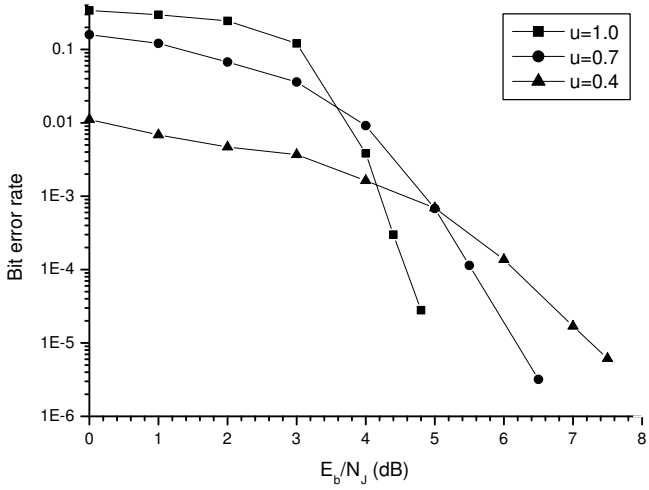

Figure 5.9: AJ performance of an IIR-filtered turbo coded DPSK system; interleaver size 400, $E_b/N_0 = 15$ dB.

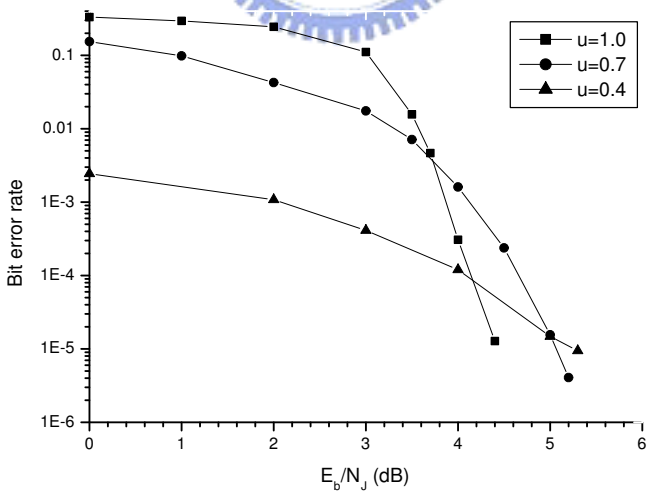

Figure 5.10: AJ performance of an IIR-filtered turbo coded DPSK system; interleaver size 800, $E_b/N_0 = 15$ dB.

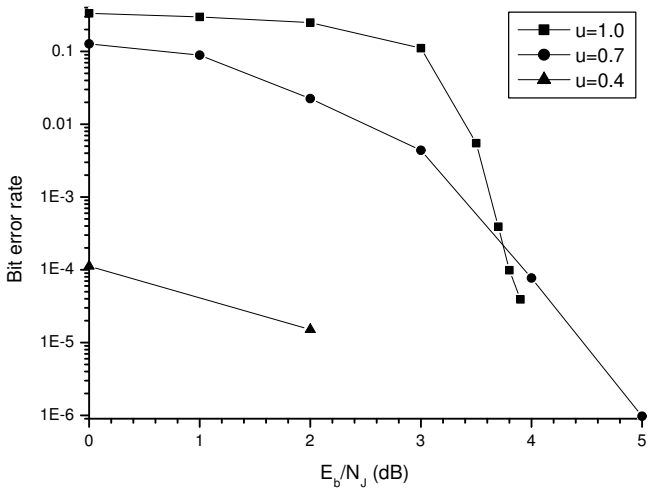

Figure 5.11: AJ performance of an IIR-filtered turbo coded DPSK system; interleaver size 1600, $E_b/N_0 = 15$ dB.

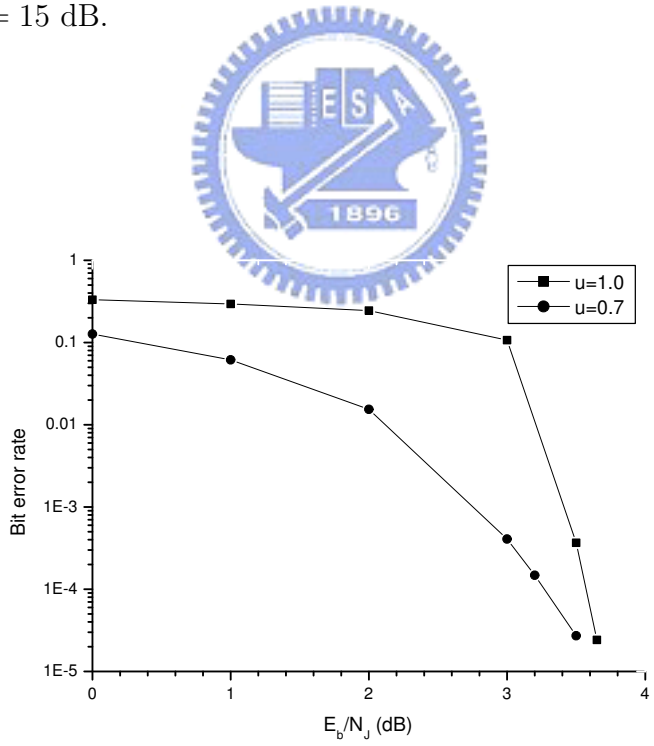

Figure 5.12: AJ performance of an IIR-filtered turbo coded DPSK system; interleaver size 3200, $E_b/N_0 = 15$ dB.

5.2.3 IBPTC coded FH/DPSK systems

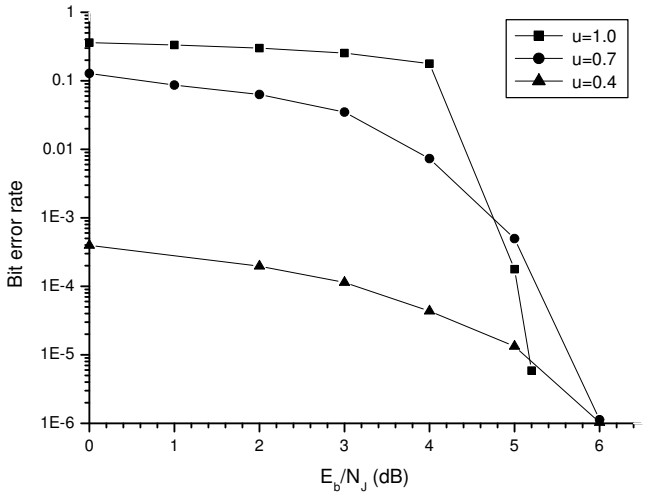

Figure 5.13: AJ performance of an IBPTC coded DPSK system; interleaver size 400, $E_b/N_0 = 15$ dB.

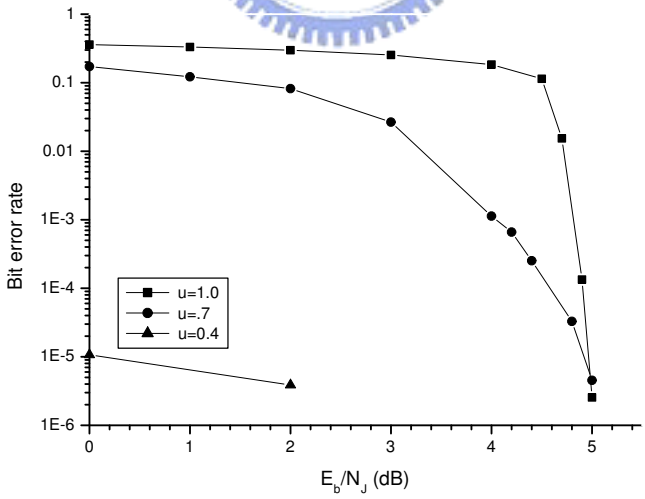

Figure 5.14: AJ performance of an IBPTC coded DPSK system; interleaver size 800, $E_b/N_0 = 15$ dB.

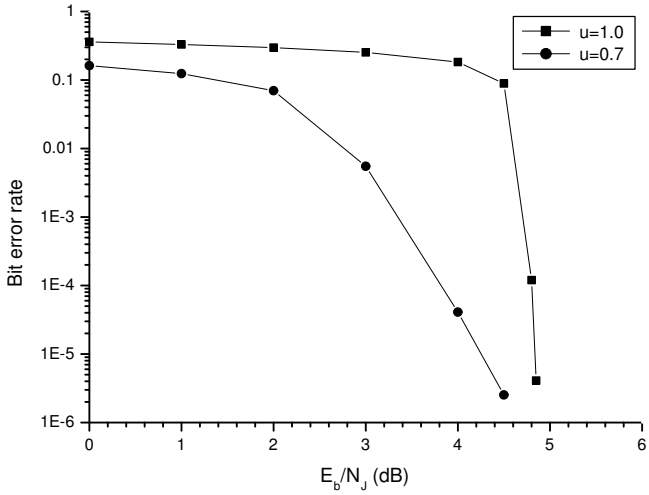

Figure 5.15: AJ performance of an IBPTC coded DPSK system; interleaver size 1600, $E_b/N_0 = 15$ dB.

5.2.4 IIR-filtered IBPTC coded FH/DPSK systems

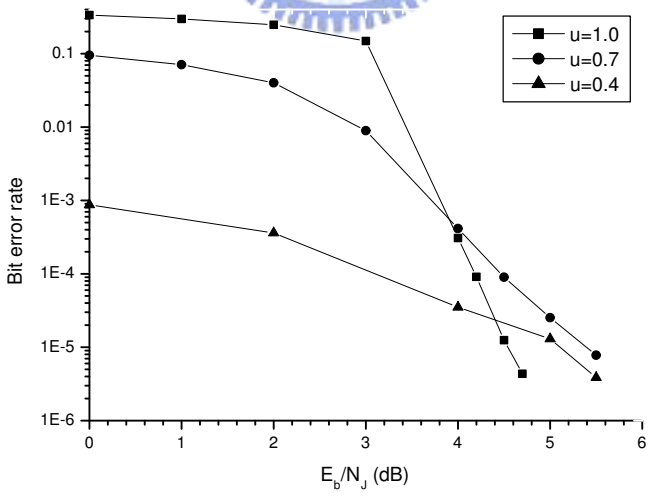

Figure 5.16: AJ performance of an IIR-filtered IBPTC coded DPSK system; interleaver size 400, $E_b/N_0 = 15$ dB.

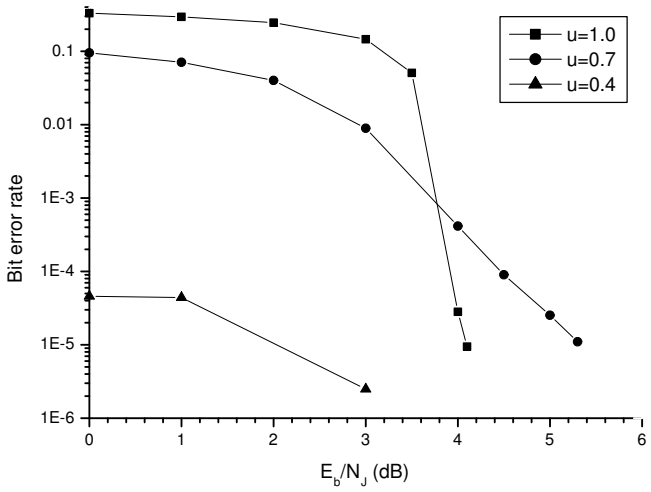

Figure 5.17: AJ performance of an IIR filtered IBP turbo coded DPSK system; interleaver size 800, $E_b/N_0 = 15$ dB.

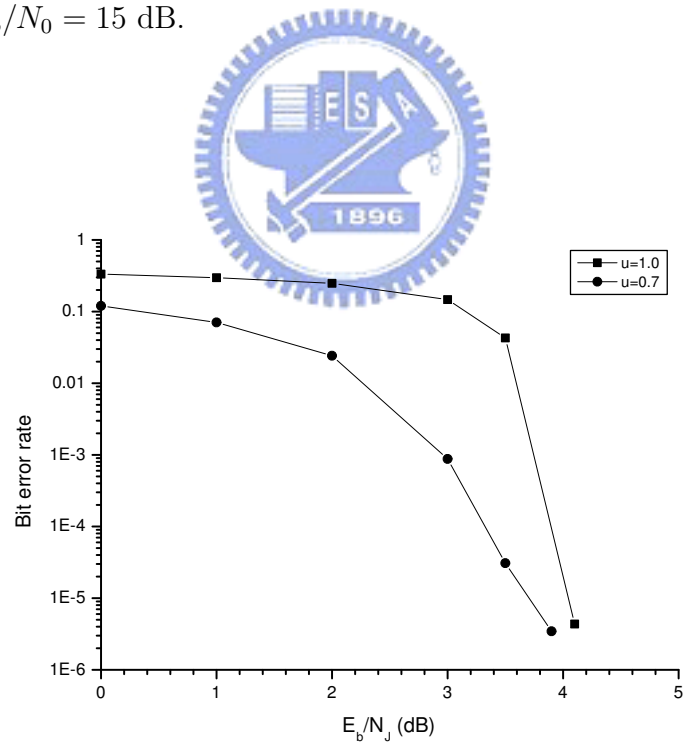

Figure 5.18: AJ performance of an IIR filtered IBP turbo coded DPSK system; interleaver size 1600, $E_b/N_0 = 15$ dB.

Chapter 6

Nonlinear Effects and Repeater Transponder

Satellite repeaters can be simply classified as regenerative repeaters and non-regenerative repeaters. A regenerative repeater regenerates, that is, demodulates and decodes the uplink signal. The regenerated bit stream is then re-encoded and re-modulated for downlink transmission. The downlink modulation and encoding can be independent of the uplink format; the re-encoding part can also be by-passed. Our previous discussion concentrates on the re-generative repeater structure and performance. A simpler and perhaps more robust satellite transponder is the bent-pipe (or non-processing) repeater. Such a satellite repeater simply transmit the received and filtered signal with a translation in carrier frequency. It is compatible with many different modulation formats (simultaneously or sequentially without any switching). A regenerative (processing) repeater, however, is usually designed to operate with only one or very few modulation formats.

The end-to-end BER performance of a processing satellite system can be estimated based on the uplink BER and downlink BER performance. When analyzing the BER performance of a bent-pipe satellite system, we should take the nonlinear effect into consideration.

6.1 Processing satellite systems

A link analysis for a on-board processing satellite system treats the uplink and downlink as two separate point-to-point links. Fig. 6.1 shows a complete satellite link with an on-board processing satellite. To calculate the overall BER performance, it is necessary to determine separately the BERs of the uplink and downlink, respectively. The bit decision at the receive ground terminal will be correct if either the bit decisions are correct on both uplink and downlink or if they are wrong on both links. Thus the probability that a bit is correctly decoded in the end-to-end link is

$$P_c = (1 - P_u)(1 - P_d) + P_u P_d \tag{6.1}$$

and the corresponding bit error probability is

$$P_e = 1 - P_c = P_u + P_d - 2P_u P_d \tag{6.2}$$

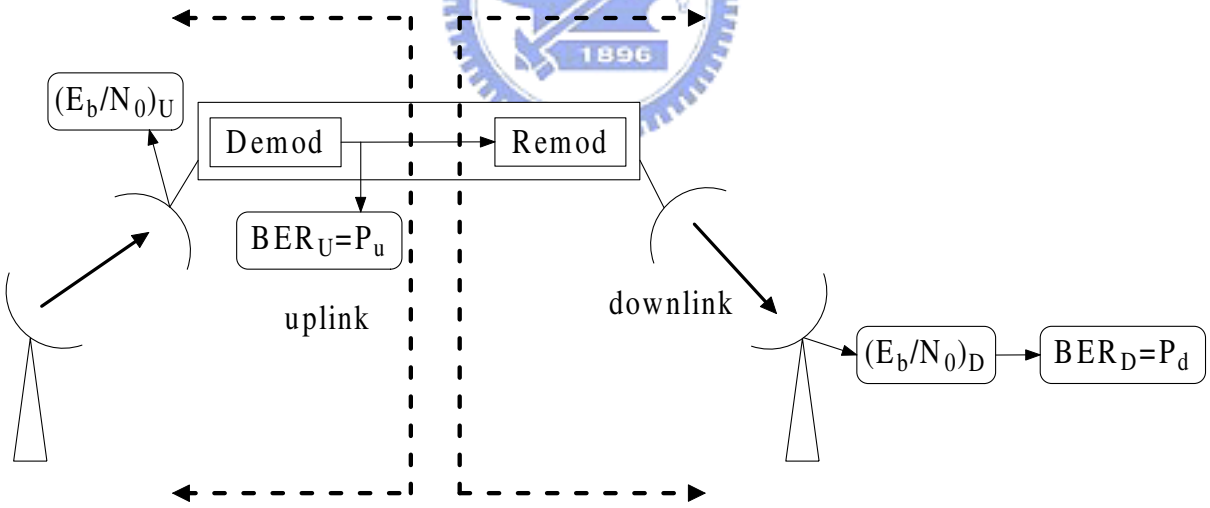

Figure 6.1: A satellite link with an on-board processing repeater.

where P_u is the probability that a is error on the uplink and P_d is the probability that a is error on the downlink. And we should assume that the channel interleaver is good enough that the error bits are uniformly distributed in a information block so

that burst error rarely happens. For very small values of P_u and P_d, the overall bit error probability can be simply approximated by summing the individual uplink and downlink bit error probabilities

$$P_e \approx P_u + P_d \tag{6.3}$$

6.2 Bent-pipe satellite systems

Link analysis for a bent-pipe satellite system treats the entire *trip* (uplink transmission to the satellite and downlink retransmission to an earth terminal) as a single link. Features that are unique to a bent-pipe satellite system, are the dependence of the overall SNR on the uplink SNR and the sharing the repeater downlink power in proportion to the uplink power from the uplink signals and noise. A bent-pipe satellite system is limited in transmission capability by its downlink power, the earth uplink terminal power, satellite and earth terminal noise and channel bandwidth. Power is severely limited in most satellite communication systems, and the inefficiencies associated with linear power amplifier stages are expensive to bear. Thus many satellite repeaters employ *nonlinear amplifiers* and the cost of signal distortion is obtained. Travelling wave tube amplifier (TWTA) is a commonly used high power amplifier in satellite systems.

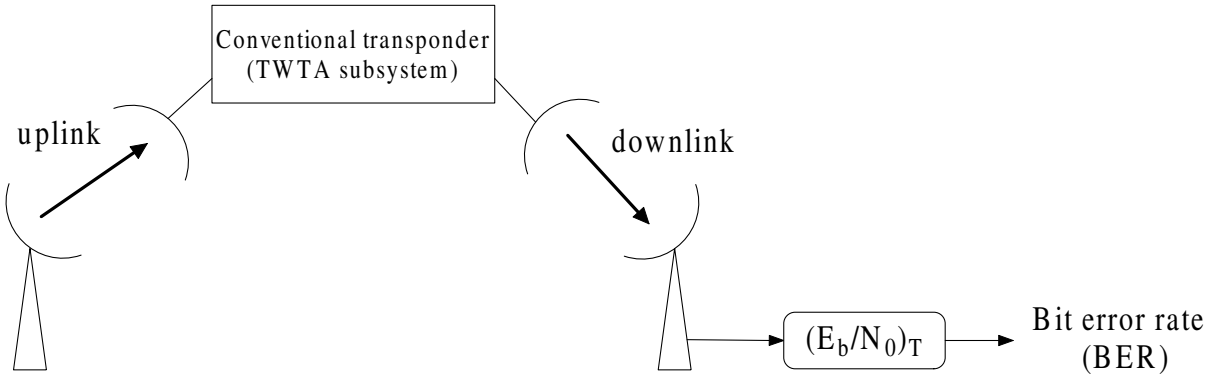

Figure 6.2: A bent-pipe satellite link.

The performance of the link is measured in terms of the BER at the output of the

earth station demodulator (decoder). The BER performance will be a function of the overall SNR $(E_b/N_0)_T$ of the complete trip. It is known that the station-to-station link SNR can be given by the expression

$$(E_b/N_0)_T^{-1} = (E_b/N_0)_u^{-1} + (E_b/N_0)_d^{-1} \tag{6.4}$$

where $(E_b/N_0)_u$ is the uplink SNR and $(E_b/N_0)_d$ is the downlink SNR.

6.2.1 TWTA subsystems

For a constant-amplitude input carrier there is a direst gain conversion to the out amplitude. As the input amplitude increases, a direct linear gain occurs in output power until the output power reaches to the point that further increase in input power no longer produces larger outputs due to a saturation effect within cavity. Achievement of this maximum output power is therefore accompanied by a nonlinear amplification with the amplifier as the saturation condition is approached.

Input saturation power (P_{in}^{sat}) is the input power that drive the output power to saturation. The ratio of P_{in}^{sat} to desired average input power P_{in} is called amplifier input backoff (IBO).

$$IBO = 10\log\left(\frac{P_{in}^{sat}}{P_{in}}\right)(dB). \tag{6.5}$$

On the other hand, the output backoff (OBO) is

$$OBO = 10\log\left(\frac{P_{out}^{sat}}{P_{out}}\right)(dB). \tag{6.6}$$

where P_{out} is the average output power and P_{out}^{sat} is the saturation output power. Therefore proper input power control is important in TWTA subsystem operations. Fig. 6.3 shows the block diagram of a power controled TWTA subsystem.

6.2.1.1 Bandpass limiter effect

In Fig. 6.3 we can see that a bandpass limiter (BPL) consists of a hard limiter followed by a bandpass filter tuned to the input carrier frequency. A BPL is often used

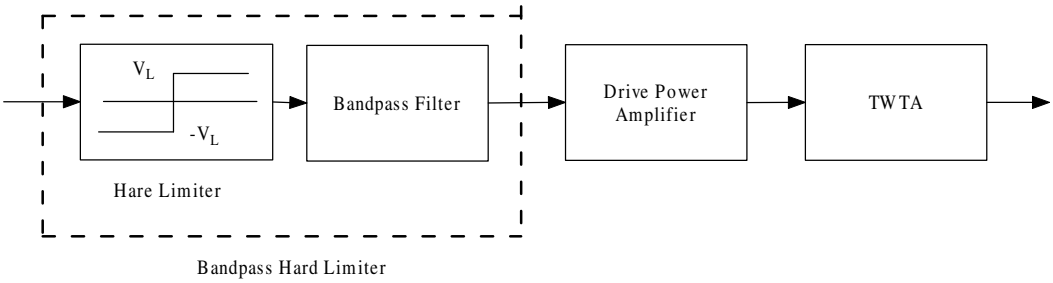

Figure 6.3: Block diagram of a TWTA subsystem.

to control the operating point of the HPAhigh power amplifier (HPA) because its a much easier device than a automatic gain control (AGC) circuit that otherwise needed.

To model the limiter effect on the input waveform, we consider the limiter input to be

$$x(t) = A\cos[\,\omega_c t + \theta(t)] + n(t) \tag{6.7}$$

an angle modulated carrier with Gaussian noise of power $R_n(0)$. Because the carrier to noise power ratio (CNR) will be altered by the limiter, we can account the effect by writing the BPL output as

$$x_L(t) = (\alpha_s A)\cos[\,\omega_c t + \theta(t)] + \alpha_n n(t) \tag{6.8}$$

where α_s and α_n represent the effective limiter *suppression factors* induced on the input carrier and noise by the limiter. The total output power of the BPL is always given by

$$P_L = \frac{1}{2}\left(\frac{4V_L}{\pi}\right) = \frac{8V_L^2}{\pi^2} \tag{6.9}$$

When the input to the BPL is composed of the sum of an phase modulated carrier and additive receiver noise, it is often desired to know the extent by which the carrier waveform has been preserved in passing through the BPL. It had been shown that the carrier power in the first harmonic term of the limiter output is given by

$$P_{cO} = \frac{2V_L^2}{\pi}\rho_i e^{-\rho_i}\left[I_0\left(\frac{\rho_i}{2}\right) + I_1\left(\frac{\rho_i}{2}\right)\right]^2 \tag{6.10}$$

where $\rho_i \triangleq \left(\frac{\alpha_s^2}{\alpha_n^2}\right)$ is the limiter input CNR.

The output noise power is

$$P_{nO} = P_L - P_{cO} \tag{6.11}$$

Then the BPL output CNR is

$$CNR_{BL} = \frac{P_{cO}}{P_{nO}} = \frac{\alpha_s^2 A^2/2}{\alpha_n^2 R_n(0)} = \frac{P_{cO}/P_L}{1-(P_{cO}/P_L)} \tag{6.12}$$

where

$$\frac{P_{cO}}{P_L} = \left(\frac{\pi}{4}\right)\rho_i e^{-\rho_i}\left[I_0\left(\frac{\rho_i}{2}\right) + I_1\left(\frac{\rho_i}{2}\right)\right]^2 \tag{6.13}$$

Fig. 6.4 is the plot of the normalized ratio

$$\Gamma \triangleq \frac{CNR_{BL}}{\rho_i} = \left(\frac{\alpha_s^2}{\alpha_n^2}\right) \tag{6.14}$$

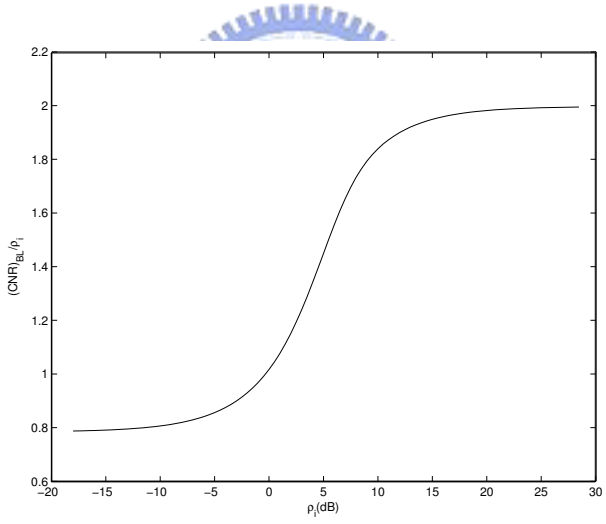

Figure 6.4: BPL CNR suppression ratio

Thus if the input CNR is large the effect of BPL cause an increase in the CNR but it cause a slight degradation by about 2 dB if the input CNR is low.

6.2.1.2 TWTA AM/AM and AM/PM distortion

TWTA is a nonlinear amplifier introducing nonlinear distortion in both the amplitude and phase. These nonlinear effects are called AM/AM and AM/PM distortions

and can be dicribed mathematically. Let the TWTA input signal be

$$s(t) = r(t)cos[\omega_c t + \varphi(t)] \tag{6.15}$$

whe ω_c is the carrier frequency and $r(t)$ and $\varphi(t)$ are the modulated envelope and phase, respectively. The corresponding output is

$$y(t) = A[r(t)]cos\omega_c t + \varphi(t) + \Phi[r(t)] \tag{6.16}$$

where $A[r(t)]$ accounts for the AM/AM effect while $\Phi[r(t)]$ represents the AM/PM effect. A simple two-parameter model was presented by Saleh [10] to model these effects. The two formulae to describe the AM/AM and AM/PM effects are

$$A[r] = \alpha_a r/(1+\beta_a r^2) \tag{6.17}$$

$$\Phi[r] = \alpha_\phi r^2/(1+\beta_\phi r^2) \tag{6.18}$$

where α_a, β_a, α_ϕ and β_ϕ are constant values depending on the TWTA used. Numerical results show that the very approximation can be obtained with proper selection of these parameters. We will use Saleh's model in our simulation as the true HPA.

In Fig. 6.5 $A(r)$ and $\Phi(r)$ are plotted for $\alpha_a = 1.9638$, $\beta_a = 0.9945$, $\alpha_\phi = 2.5293$ and $\beta_\phi = 2.8167$.

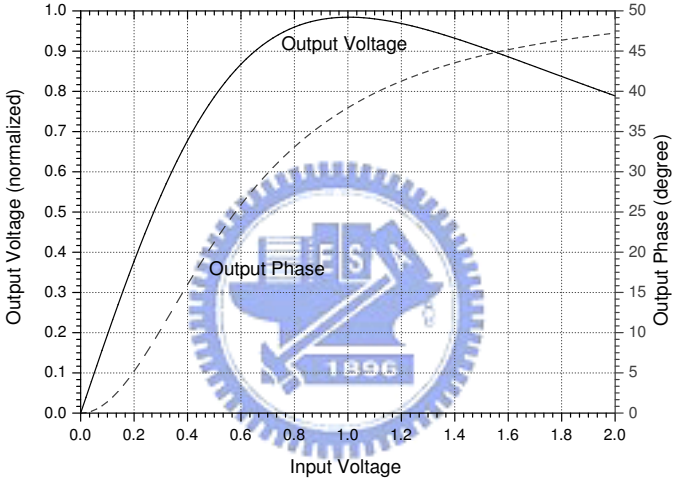

Figure 6.5: Typical TWTA AM/AM and AM/PM distortion characteristic (normalized).

Chapter 7

End-to-End Link Performance

In this chapter, we present end-to-end link performance of the four receiver structures discussed before for both bent-pipe and processing satellite systems. They are (1) turbo coded DPSK, (2) IBPTC coded DPSK, (3) IIR-filtered turbo coded DPSK and (4) IIR-filtered IBPTC coded DPSK systems.

7.1 AJ performance of bent-pipe satellite systems

This section summarizes the performance of the four receiver structures with proper interleaver sizes. The uplink communication channel contains PBNJ and AWGN background noise and the downlink is corrupted by AWGN only. The complete link E_b/N_0 is 15 dB or 10 dB, that is,

$$(E_b/N_0)_T^{-1} = (E_b/N_0)_u^{-1} + (E_b/N_0)_d^{-1}.$$

Since the amplifier of the ground transmit station can always provide signal power larger than that of a satellite repeater the uplink SNR can always be made greater than the downlink SNR. The uplink and downlink SNR distribution considered in our simulations are: $(E_b/N_0)_u = (E_b/N_0)_d$ and $(E_b/N_0)_u = 10(E_b/N_0)_d$. Table 7.1 and Table 7.2 list the actually values of uplink and downlink SNRs.

The worst case performance is given in Table 7.3 and Table 7.4. One can easily see that both cases, $(\frac{E_b}{N_0})_u = (\frac{E_b}{N_0})_d$ and $(\frac{E_b}{N_0})_u = 10(\frac{E_b}{N_0})_d$, yield almost the same performance

Table 7.1: Uplink and downlink SNR distribution ($(E_b/N_0)_T = 10$ dB).

$(E_b/N_0)_T$=10dB	$(E_b/N_0)_u$	$(E_b/N_0)_d$
$(E_b/N_0)_u = (E_b/N_0)_d$	13 dB	13 dB
$(E_b/N_0)_u = 10(E_b/N_0)_d$	20.41 dB	10.41 dB

Table 7.2: Uplink and downlink SNR distribution ($(E_b/N_0)_T = 15$ dB).

$(E_b/N_0)_T$=15dB	$(E_b/N_0)_u$	$(E_b/N_0)_d$
$(E_b/N_0)_u = (E_b/N_0)_d$	18 dB	18 dB
$(E_b/N_0)_u = 10(E_b/N_0)_d$	25.41 dB	15.41 dB

when the jamming probability is high (100% and 70%). In such a case, the uplink jamming noise is suppressed after passing through the BPL (Fig. 6.4), therefore the performance is dominated by the value of E_b/N_J. When the jamming probability is low ($< 40\%$), the case $(\frac{E_b}{N_0})_u = (\frac{E_b}{N_0})_d$ outperforms the other case– $(\frac{E_b}{N_0})_u = 10(\frac{E_b}{N_0})_d$. This is because when the jamming probability is low, the jamming power is significant larger once a hopping block is jammed thus the overall noise will be enhanced even E_b/N_J is large, therefore the BER performance are dominated by the downlink SNR. The downlink SNR of $(\frac{E_b}{N_0})_u = (\frac{E_b}{N_0})_d$ case is higher than that of $(\frac{E_b}{N_0})_u = 10(\frac{E_b}{N_0})_d$ case, thus the $(\frac{E_b}{N_0})_u = (\frac{E_b}{N_0})_d$ curve performs better than the $(\frac{E_b}{N_0})_u = 10(\frac{E_b}{N_0})_d$ curve in low jamming probability case.

Both of two receiver structures–IIR filtered turbo coded FH/DPSK with 3200 interleaver size and IIR-filtered IBPTC coded FH/DPSK with 1600 interleaver size–can force the jammer to jam the full band and the former outperforms the former structure.

Table 7.3: Worst case performance comparison of bent-pipe satellite systems with $(E_b/N_0)_T = 10$ dB).

system structure (interleaver size)	$(\frac{E_b}{N_0})_u = (\frac{E_b}{N_0})_d$	$(\frac{E_b}{N_0})_u = 10(\frac{E_b}{N_0})_d$
turbo coded FH/DPSK (3200)	6.5 dB	6.5 dB
IIR filtered turbo coded FH/DPSK (3200)	5.2 dB	5.2 dB
IBP turbo coded FH/DPSK (1600)	6.05 dB	5.95 dB
IIR filtered IBP turbo coded FH/DPSK(1600)	5.15 dB	5.05 dB

Table 7.4: Worst case performance comparison of bent-pipe satellite systems with $(E_b/N_0)_T = 15$ dB).

system structure (interleaver size)	$(\frac{E_b}{N_0})_u = (\frac{E_b}{N_0})_d$	$(\frac{E_b}{N_0})_u = 10(\frac{E_b}{N_0})_d$
turbo coded FH/DPSK (3200)	5.5 dB	5.5 dB
IIR filtered turbo coded FH/DPSK (3200)	4.15 dB	4.2 dB
IBP turbo coded FH/DPSK (1600)	5.1 dB	5.1 dB
IIR filtered IBP turbo coded FH/DPSK(1600)	4.4 dB	4.3 dB

7.1.1 Turbo coded FH/DPSK systems

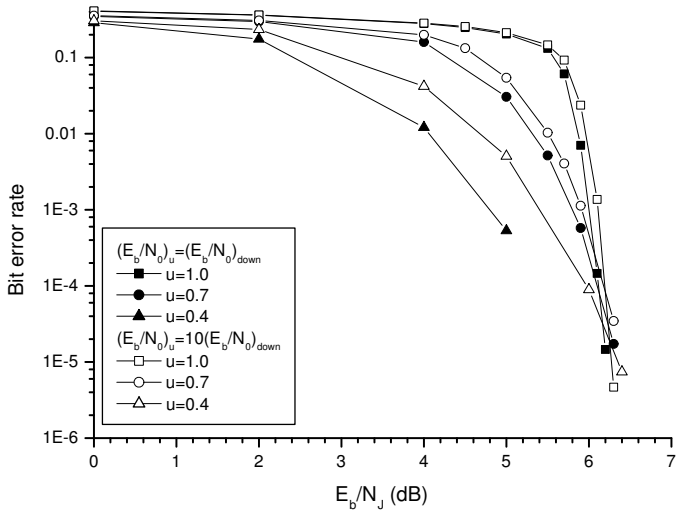

Figure 7.1: AJ performance of a turbo coded DPSK nonlinear satellite system; interleaver size 3200, $(E_b/N_0)_t = 10$ dB and multihop SNR Estimator C.

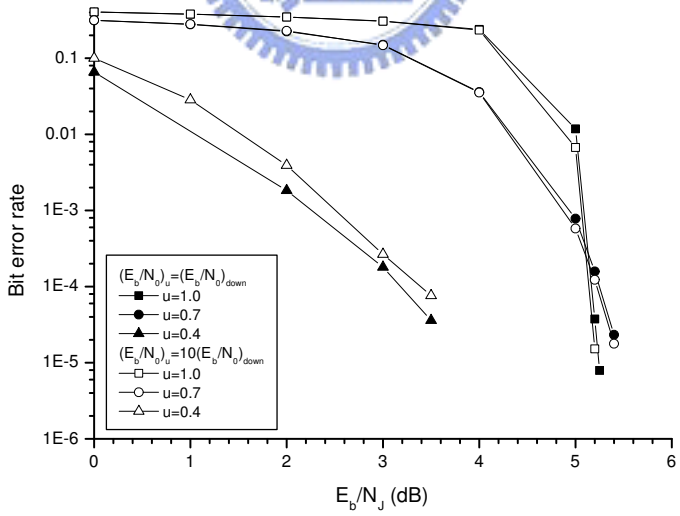

Figure 7.2: AJ performance of a turbo coded DPSK nonlinear satellite system; interleaver size 3200, $(E_b/N_0)_t = 15$ dB and multihop SNR Estimator C.

7.1.2 IIR-filtered turbo coded FH/DPSK systems

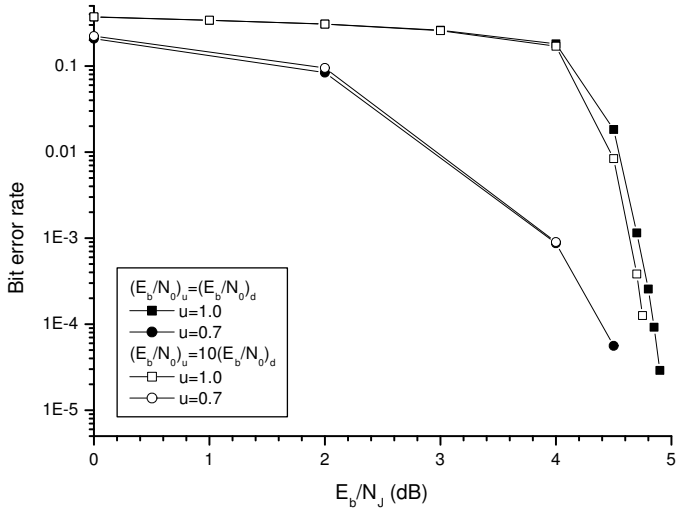

Figure 7.3: AJ performance of an IIR-filtered turbo coded DPSK nonlinear satellite system with interleaver size 3200, $(E_b/N_0)_t = 10$ dB and multihop SNR Estimator C.

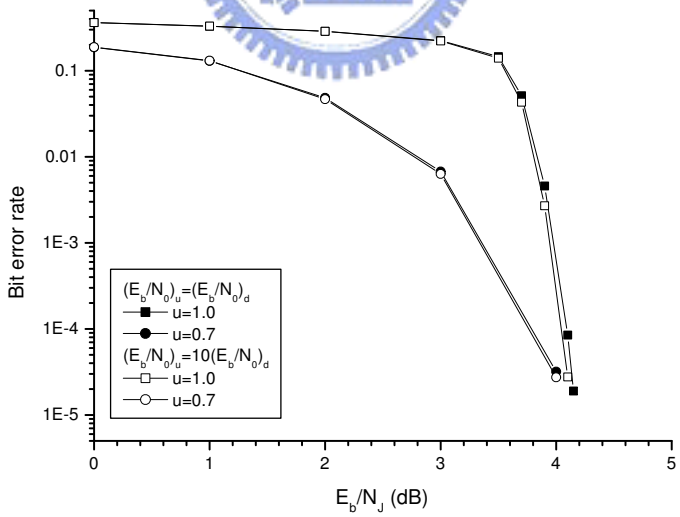

Figure 7.4: AJ performance of an IIR-filtered turbo coded DPSK nonlinear satellite system with interleaver size 3200, $(E_b/N_0)_t = 15$ dB and multihop SNR Estimator C.

7.1.3 IBPTC coded FH/DPSK systems

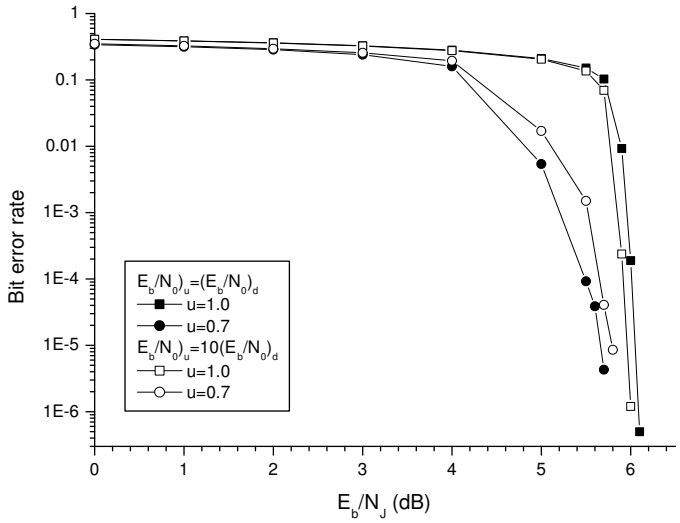

Figure 7.5: AJ performance of an IBPTC coded DPSK nonlinear satellite system with interleaver size 1600, $(E_b/N_0)_t = 10$ dB and multihop SNR Estimator C.

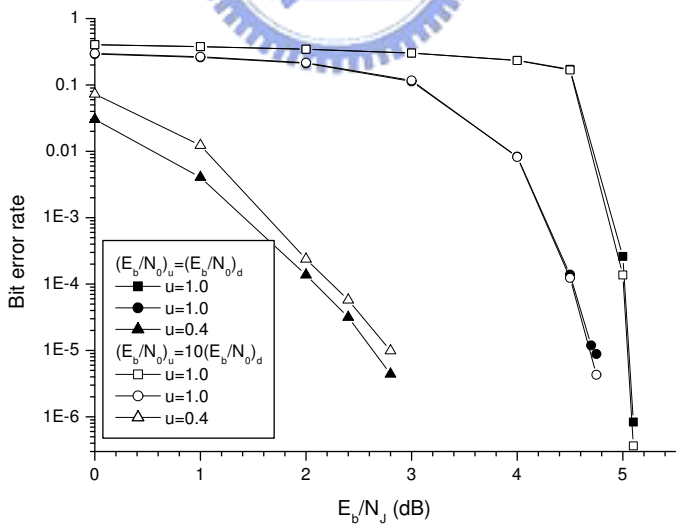

Figure 7.6: AJ performance of an IBPTC coded DPSK nonlinear satellite system with interleaver size 1600, $(E_b/N_0)_t = 15$ dB and multihop SNR Estimator C.

7.1.4 IIR-filtered IBPTC coded FH/DPSK systems

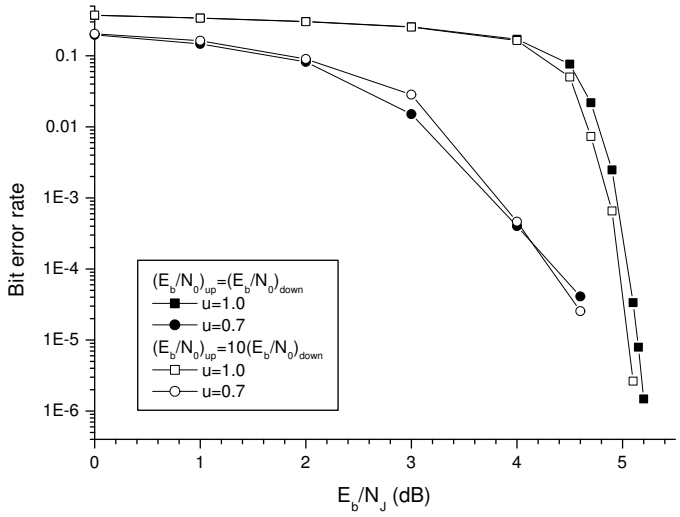

Figure 7.7: AJ performance an IIR-filtered IBPTC coded DPSK nonlinear satellite system with interleaver size 1600, $(E_b/N_0)_t = 10$ dB and multihop SNR Estimator C.

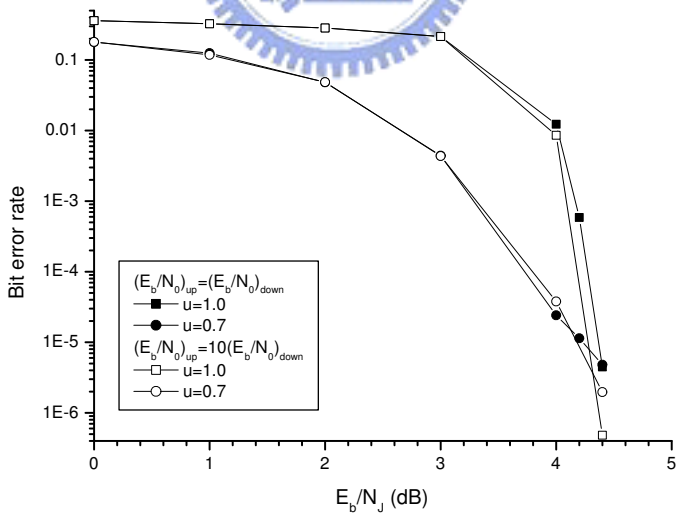

Figure 7.8: AJ performance an IIR-filtered IBPTC coded DPSK nonlinear satellite system with interleaver size 1600, $(E_b/N_0)_t = 10$ dB and multihop SNR Estimator C.

7.2 AJ performance of processing satellite systems

We present the AJ performance of a processing satellite system with uplink background AWGN noise $(E_b/N_0)_u = 13$ dB and 18 dB for the same four receiver structures. We assume the rate 1/2 {554,744} convolutional code is employed in the downlink. The end-to-end link performance is evaluated according to

$$P_e \approx P_u + P_d.$$

We further assume that downlink bit stream is interleaved before re-encoding such that no burst error in the re-coded bit stream.

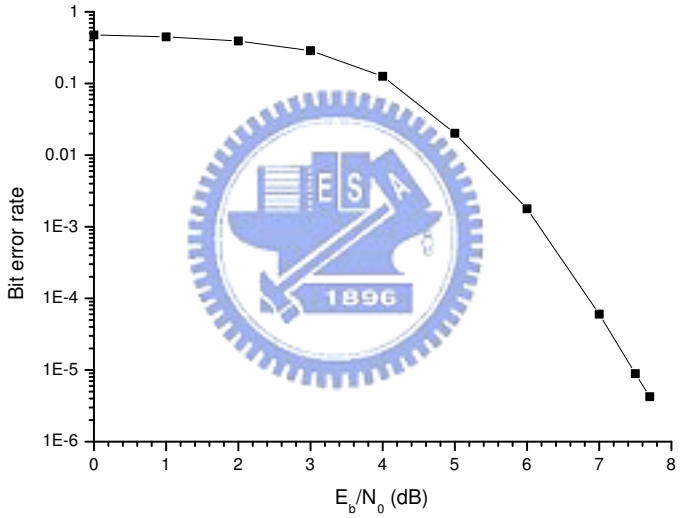

Figure 7.9: BER performance of the rate 1/2, {554,744} convolutional code in an AWGN channel.

Table 7.5: Worst case performance comparison of bent-pipe satellite systems.

$(E_b/N_0)_T$ 10dB	required $(E_b/N_J)_u$	$(E_b/N_0)_u$	$(E_b/N_0)_u$
turbo coded FH/DPSK (3200)	6.5 dB	13 dB	13 dB
IIR filtered turbo coded FH/DPSK (3200)	5.2 dB	13 dB	13 dB
IBP turbo coded FH/DPSK (1600)	6.05 dB	13 dB	13 dB
IIR filtered IBP turbo coded FH/DPSK(1600)	5.15 dB	13 dB	13 dB
$(E_b/N_0)_T$ 15dB	required $(E_b/N_J)_u$	$(E_b/N_0)_u$	$(E_b/N_0)_u$
turbo coded FH/DPSK (3200)	5.5 dB	18 dB	18 dB
IIR filtered turbo coded FH/DPSK (3200)	4.15 dB	18 dB	18 dB
IBP turbo coded FH/DPSK (1600)	5.1 dB	18 dB	18 dB
IIR filtered IBP turbo coded FH/DPSK(1600)	4.4 dB	18 dB	18 dB

Table 7.6: Worst case performance comparison of processing satellite systems.

$(E_b/N_0)_T$ 10dB	required $(E_b/N_J)_u$	$(E_b/N_0)_u$	$(E_b/N_0)_u$
turbo coded FH/DPSK (3200)	5.8 dB	13 dB	7.5 dB
IIR filtered turbo coded FH/DPSK (3200)	4.4 dB	13 dB	7.5 dB
IBP turbo coded FH/DPSK (1600)	5.4 dB	13 dB	7.5 dB
IIR filtered IBP turbo coded FH/DPSK(1600)	4.6 dB	13 dB	7.5 dB
$(E_b/N_0)_T$ 15dB	required $(E_b/N_J)_u$	$(E_b/N_0)_u$	$(E_b/N_0)_u$
turbo coded FH/DPSK (3200)	5.2 dB	18 dB	7.5 dB
IIR filtered turbo coded FH/DPSK (3200)	4 dB	18 dB	7.5 dB
IBP turbo coded FH/DPSK (1600)	5 dB	18 dB	7.5 dB
IIR filtered IBP turbo coded FH/DPSK(1600)	4.2 dB	18 dB	7.5 dB

7.2.1 Turbo coded FH/DPSK systems

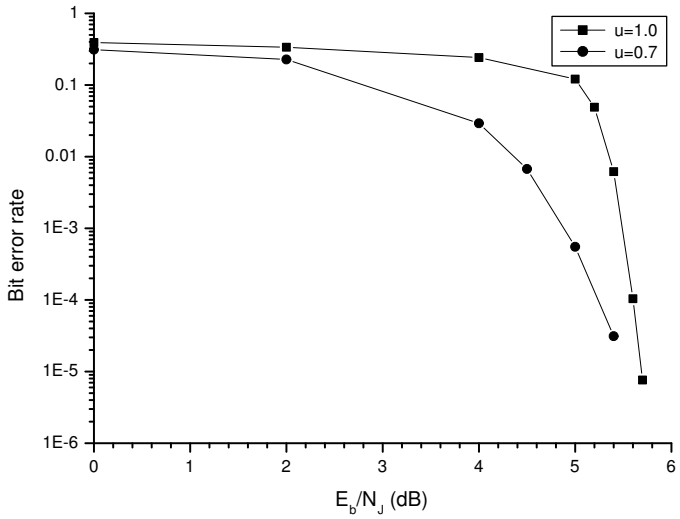

Figure 7.10: Uplink AJ performance of a turbo coded DPSK system; interleaver size 3200, $(E_b/N_0)_u = 13$ dB, multihop SNR Estimator C.

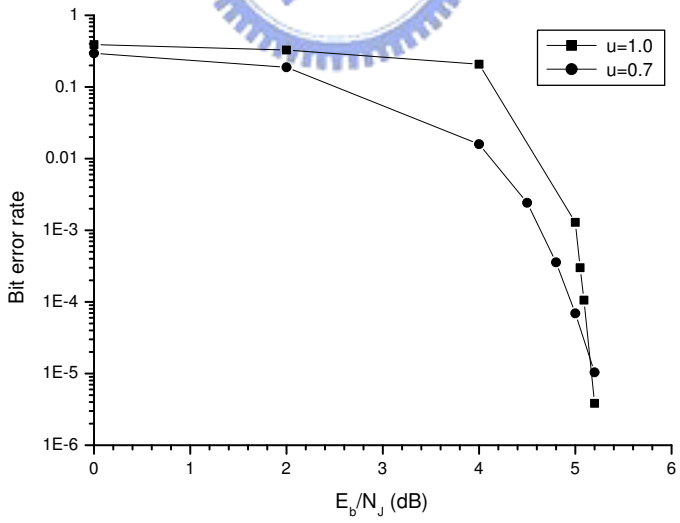

Figure 7.11: Uplink AJ performance of a turbo coded DPSK system; interleaver size 3200, $(E_b/N_0)_u = 18$ dB, multihop SNR Estimator C.

7.2.2 IIR -filtered turbo coded FH/DPSK systems

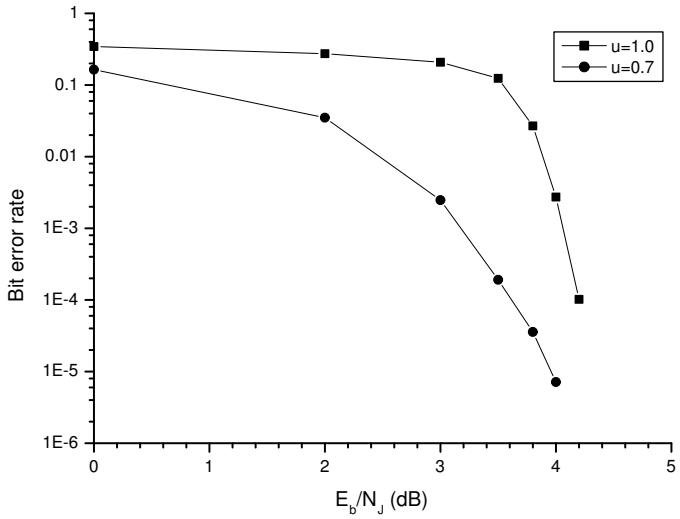

Figure 7.12: Uplink AJ performance of an IIR-filtered turbo coded DPSK system; interleaver size 3200, $(E_b/N_0)_u = 13$ dB, multihop SNR Estimator C.

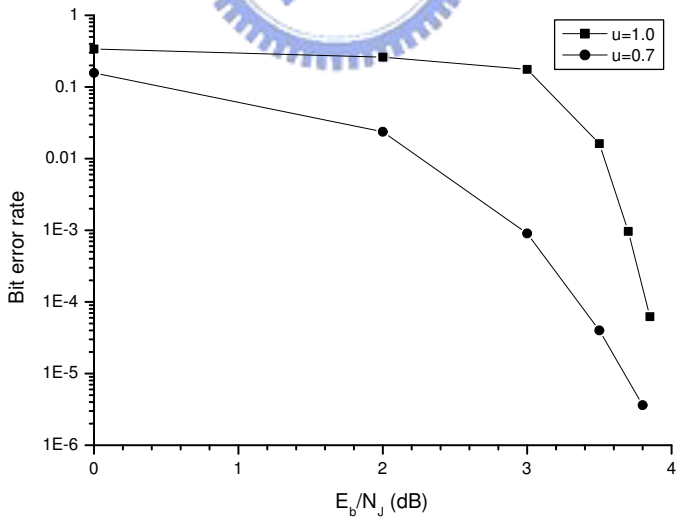

Figure 7.13: Uplink AJ performance of an IIR-filtered turbo coded DPSK system; interleaver size 3200, $(E_b/N_0)_u = 18$ dB, multihop SNR Estimator C.

7.2.3 IBPTC coded FH/DPSK systems

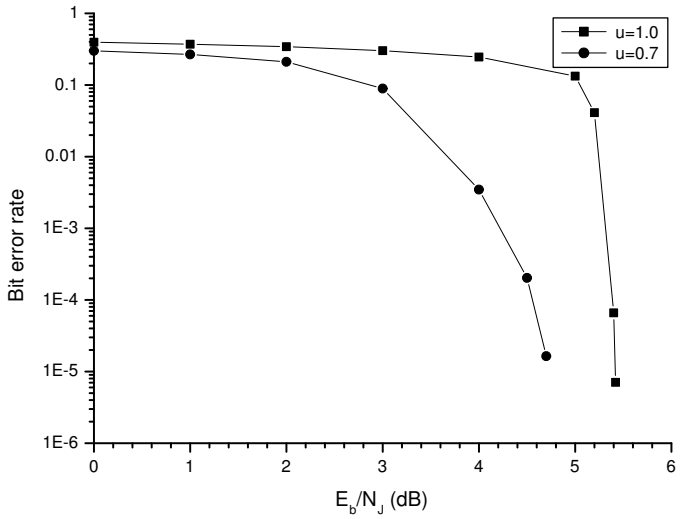

Figure 7.14: Uplink AJ performance of an IBPTC coded DPSK system; interleaver size 1600, $(E_b/N_0)_u = 13$ dB, multihop SNR Estimator C.

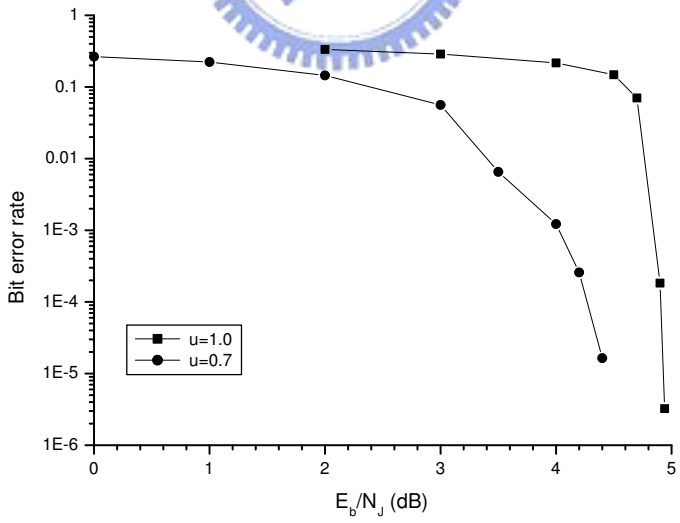

Figure 7.15: Uplink AJ performance of an IBPTC coded DPSK system; interleaver size 1600, $(E_b/N_0)_u = 18$ dB, multihop SNR Estimator C.

7.2.4 IIR-filtered IBPTC coded FH/DPSK systems

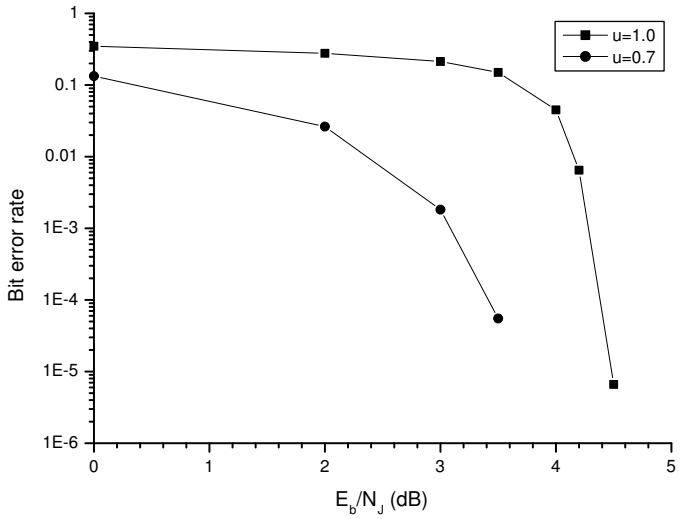

Figure 7.16: Uplink AJ performance of an IIR-filtered IBPTC coded DPSK system; interleaver size 1600, $(E_b/N_0)_u = 13$ dB, multihop SNR Estimator C.

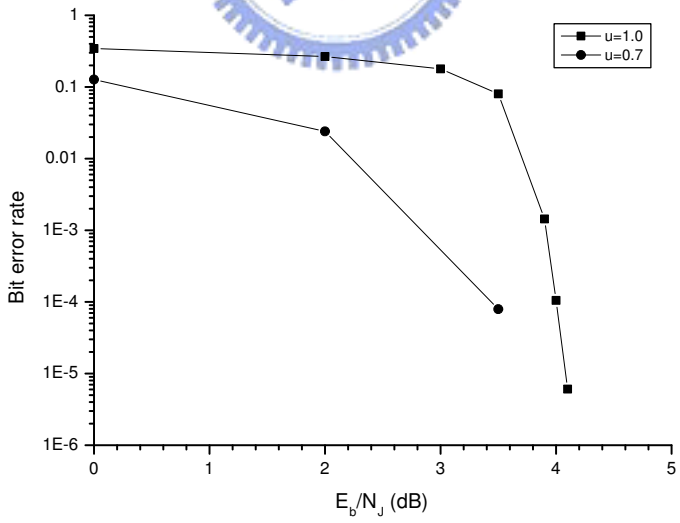

Figure 7.17: Uplink AJ performance of an IIR-filtered IBPTC coded DPSK system; interleaver size 1600, $(E_b/N_0)_u = 18$ dB, multihop SNR Estimator C.

7.3 AJ performance of very low hopping rate satellite systems

This section considers the AJ performance in a low hopping rate (1000 bits/hop) system. Previous simulations all assume a 100 bits/hop hopping rate system. The purpose is to demonstrate the usefulness of IBPTCs in combating jamming with a reduced hopping rate.

Table 7.7: Worst case performance comparison of bent-pipe satellite systems (1000 bits/hop).

$(E_b/N_0)_T$ 10dB	required $(E_b/N_J)_u$	$(E_b/N_0)_u$	$(E_b/N_0)_u$
CTC coded FH/DPSK (3200)	9.3 dB	13 dB	13 dB
IBPTC coded FH/DPSK (1600)	8.75 dB	13 dB	13 dB
$(E_b/N_0)_T$ 15dB	required $(E_b/N_J)_u$	$(E_b/N_0)_u$	$(E_b/N_0)_u$
CTC coded FH/DPSK (3200)	8.5 dB	18 dB	18 dB
IBPTC coded FH/DPSK (1600)	8.0 dB	18 dB	18 dB

Table 7.8: Worst case performance comparison of processing satellite systems (1000 bits/hop).

$(E_b/N_0)_T$ 10dB	required $(E_b/N_J)_u$	$(E_b/N_0)_u$	$(E_b/N_0)_u$
CTC coded FH/DPSK (3200)	8.75 dB	13 dB	7.5 dB
IBPTC coded FH/DPSK (1600)	8.0 dB	13 dB	7.5 dB
$(E_b/N_0)_T$ 15dB	required $(E_b/N_J)_u$	$(E_b/N_0)_u$	$(E_b/N_0)_u$
CTC coded FH/DPSK (3200)	8.3 dB	18 dB	7.5 dB
IBPTC coded FH/DPSK (1600)	7.75 dB	18 dB	7.5 dB

7.3.1 Bent-pipe turbo coded FH/DPSK systems

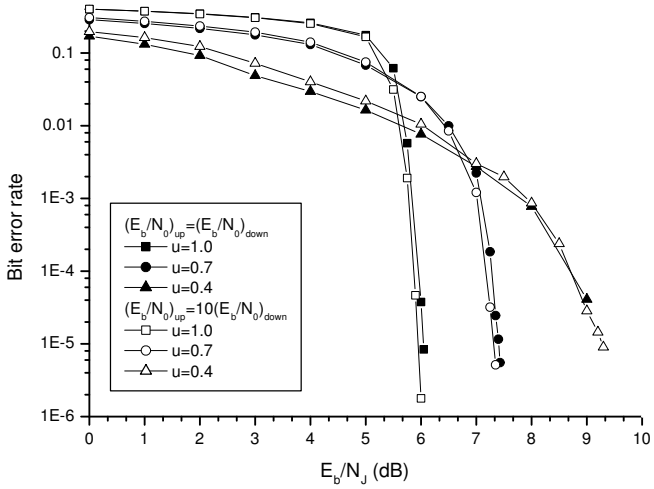

Figure 7.18: AJ performance of a turbo coded DPSK nonlinear satellite system; 1000 bits/hop, interleaver size 3200, $(E_b/N_0)_t = 10$ dB, multihop SNR Estimator C.

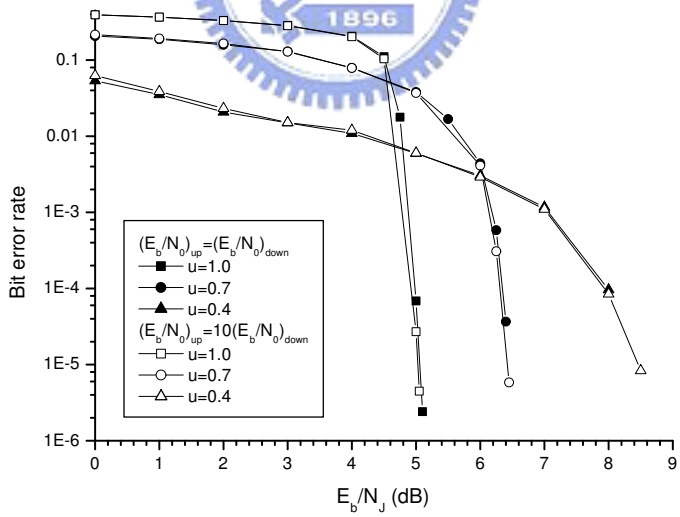

Figure 7.19: AJ performance of a turbo coded DPSK nonlinear satellite system; 1000 bits/hop, interleaver size 3200, $(E_b/N_0)_t = 15$ dB, multihop SNR Estimator C.

7.3.2 Bent-pipe IBPTC coded FH/DPSK systems

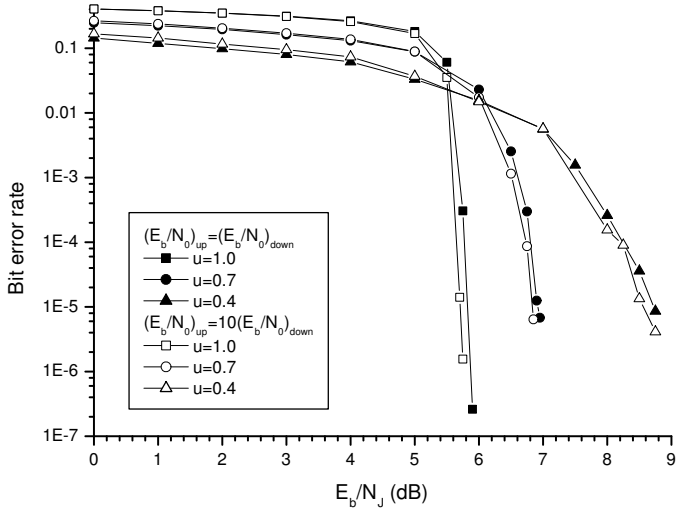

Figure 7.20: AJ performance of an IBPTC coded DPSK nonlinear satellite system; 1000 bits/hop, interleaver size 1600, $(E_b/N_0)_t = 10$ dB, multihop SNR Estimator C.

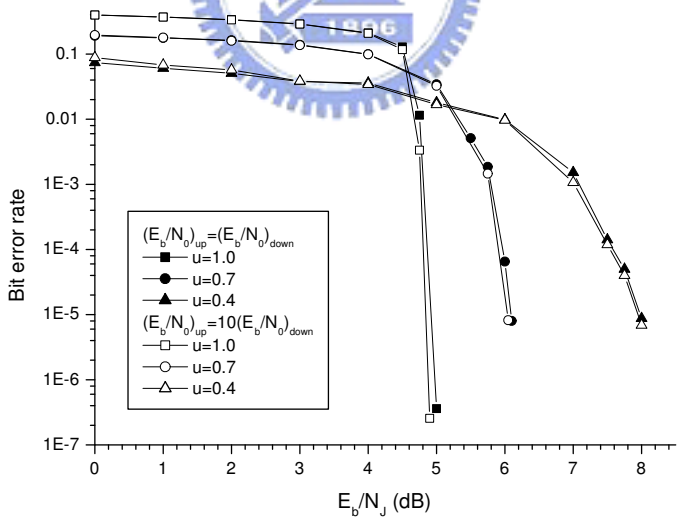

Figure 7.21: AJ performance of an IBPTC coded DPSK nonlinear satellite system; 1000 bits/hop, interleaver size 1600, $(E_b/N_0)_t = 15$ dB, multihop SNR Estimator C.

7.3.3 Turbo coded FH/DPSK system with on-board processing

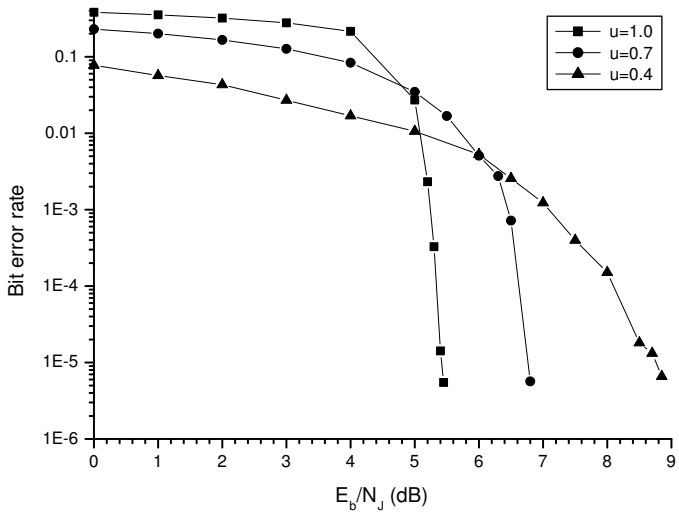

Figure 7.22: Uplink AJ performance of a turbo coded DPSK system; 1000 bits/hop, interleaver size 3200, $(E_b/N_0)_u = 13$ dB, multihop SNR Estimator C.

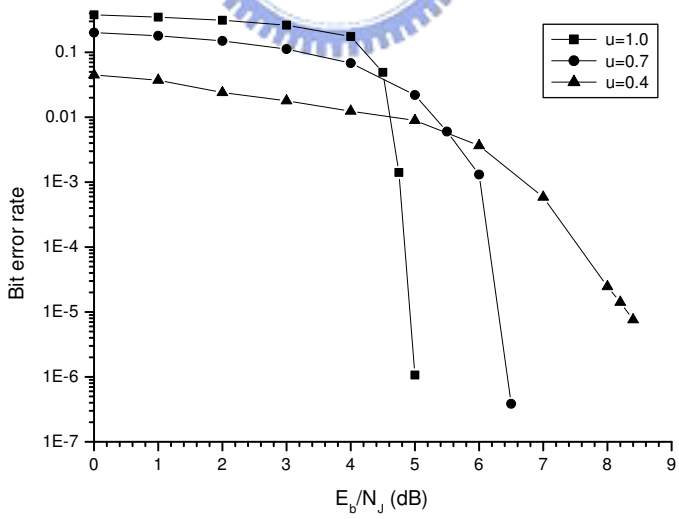

Figure 7.23: Uplink AJ performance of a turbo coded DPSK system; 1000 bits/hop, interleaver size 3200, $(E_b/N_0)_u = 18$ dB, multihop SNR Estimator C.

7.3.4 IBPTC coded FH/DPSK system with on-board processing

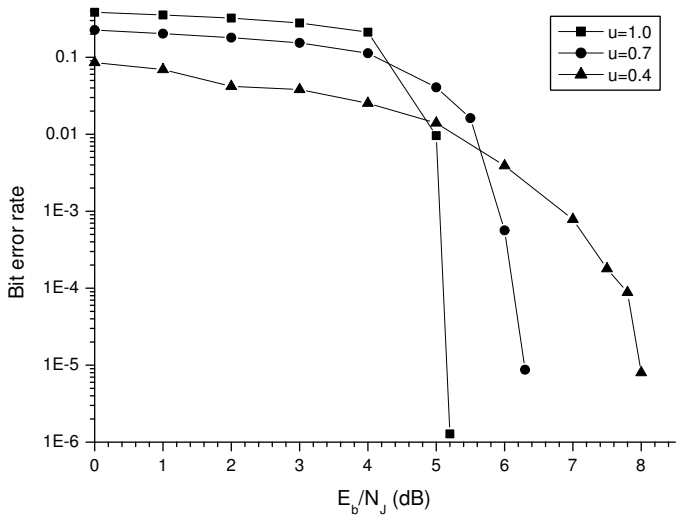

Figure 7.24: Uplink AJ performance of an IBPTC coded DPSK system; 1000 bits/hop, interleaver size 1600, $(E_b/N_0)_u = 13$ dB, multihop SNR Estimator C.

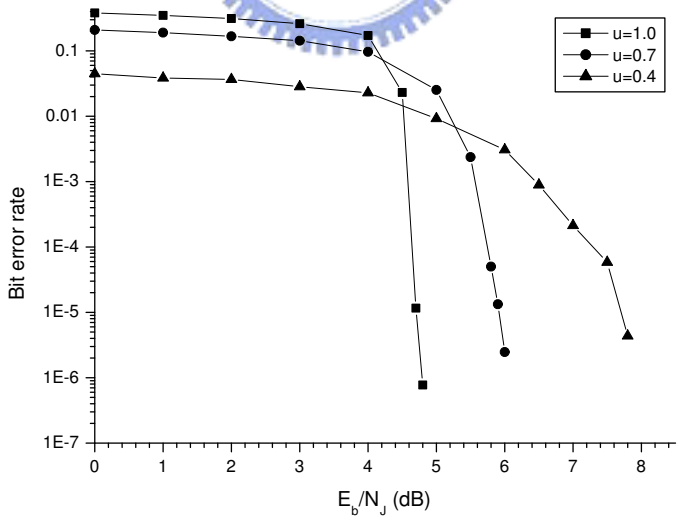

Figure 7.25: Uplink AJ performance of an IBPTC coded DPSK system; 1000 bits/hop, interleaver size 1600, $(E_b/N_0)_u = 18$ dB, multihop SNR Estimator C.

Chapter 8

Conclusion

We present four turbo coded FH/DPSK receiver structures for bent-pipe and processing satellite systems. To facilitate turbo decoding, we propose several SNR estimators and examine their effectiveness. To further improve the estimators performance, we extend these schemes to a multiple hop scenario, resulting in less than 0.3 dB performance degradation with respect to the perfect SNR estimator. Tables 8.1 and 8.2 summarize the worst case end-to-end performance of various receiver structures with both bent-pipe and on-board processing options, where $(\frac{E_b}{N_0})_u$ denotes the uplink SNR, $(\frac{E_b}{N_J})_o$ and $(\frac{E_b}{N_0})_{d,o}$ are the required SJR and downlink SNR for a processing satellite system, $(\frac{E_b}{N_J})_b$ and $(\frac{E_b}{N_0})_{d,b}$ are their counterparts for a bent-pipe satellite system.

Table 8.1: Worst case performance comparison of processing satellite systems and bent-pipe satellite systems (100 bits/hop).

	$(\frac{E_b}{N_0})_u$	$(\frac{E_b}{N_J})_o$	$(\frac{E_b}{N_0})_{d,o}$	$(\frac{E_b}{N_J})_b$	$(\frac{E_b}{N_0})_{d,b}$
turbo coded FH/DPSK	13	5.8	7.5	6.5	13
IIR filtered turbo coded FH/DPSK	13	4.4	7.5	5.2	13
IBP turbo coded FH/DPSK	13	5.4	7.5	6.05	13
IIR filtered IBP turbo coded FH/DPSK	13	4.6	7.5	5.15	13
turbo coded FH/DPSK	18	5.2	7.5	5.5	18
IIR filtered turbo coded FH/DPSK	18	4	7.5	4.15	18
IBP turbo coded FH/DPSK	18	5	7.5	5.1	18
IIR filtered IBP turbo coded FH/DPSK	18	4.2	7.5	4.4	18

These results indicate that the IBPTC option does provide sufficient coding gain in

Table 8.2: Worst case performance comparison of processing and bent-pipe satellite systems. (1000 bits/hop).

	$(\frac{E_b}{N_0})_u$	$(\frac{E_b}{N_J})_o$	$(\frac{E_b}{N_0})_{d,o}$	$(\frac{E_b}{N_J})_b$	$(\frac{E_b}{N_0})_{d,b}$
turbo coded FH/DPSK	13	8.75	7.5	9.3	13
IBP turbo coded FH/DPSK	13	8.0	7.5	8.75	13
turbo coded FH/DPSK	18	8.3	7.5	8.5	18
IBP turbo coded FH/DPSK	18	7.75	7.5	8.0	18

the low hopping rate region. Note that although a lower hopping rate causes a jammed hop to contain more contaminated samples, the decoder, through IBP interleaving, is able to import information from adjacent unjammed blocks so that the reliability of the jammed block increases. For a regenerative link, 0.55 dB to 0.8 dB gain is obtained in low uplink SNR region while only 0.1 dB to 0.3 dB is obtained in high uplink SNR region. Finally, the downlink convolutional code gives a 5.5 (10.5) dB downlink gain when $(\frac{E_b}{N_0})_u = 13(18)$ dB.

Bibliography

[1] T. Mizuochi, K. Ishida, T. Kobayashi, J. Abe, K. Kinjo, K. Motoshima, K. Kasahara, "A comparative study of DPSK and OOK WDM transmission over transoceanic distances and their performance degradations due to nonlinear phase noise," *Lightwave Technology Journal*, vol. 21, no. 9, pp. 1933-1943, Sep. 2003.

[2] C. Berrou, A. Glavieux, and P. L. Thitimajshima, "Near Shannon limit error-correcting coding and decoding: Turbo-codes," in Proc. ICC'93, pp. 1064-1070, May 1993.

[3] R. A. Williams and H. I. Paul, "Potential uses of the military Ka-band for wideband MILSATCOM systems," in Proc. MILCOM'98, Vol. 1, pp. 30-34, Oct. 1998.

[4] M. Jordan, "Turbo-code performance in partial-band jamming" in Proc. MILCOM, Oct. 1998.

[5] G. D. Forney, *Concatenated Codes*, Cambridge, MA:MIT Press, 1966.

[6] N. Hamamoto, "Differential detection with IIR filter for improving DPSK detection performance," *IEEE Trans. Commun.*, vol. 44, no. 8, Aug. 1996.

[7] TS 25.222 V3.1.1 *Multiplexing and channel coding (TDD)*, 3GPP TSG RAN WG1, Dec. 1999.

[8] Y. X. Zheng, Y. T. Su, "A new real-time MAP decoding algorithm," Proc. 2nd Inter. Sympo. Turbo Codes, pp. 507-510, Sep. 2000.

[9] Y. X. Zheng, Y. T. Su, "A new interleaver design and its application to turbo codes," Proc. VTC2002fall, VOL.3, pp.1437-1441, Sep. 2002.

[10] A. M. Saleh, "Frequency-independent and frequency-dependent nonlinear models of TWT amplifiers," *IEEE Trans. Commun.*, vol.COM-29, no. 11, Nov. 1981.

[11] T, A. Summers and S. G. Wilson, "SNR mismatch and online estimation in turbo coding," *IEEE Trans. Commun.*, vol. 46, no. 4, Apr. 1998.

[12] S. A. Siltala, "Some suboptimum turbo decoders and their sensitivity to SNR estimation using DPSK modulation," in *Proc. MILCOM 98*, vol.3, pp. 1008-1012, Oct. 1998.

[13] E. K Hall and S. G. Wilson, "Turbo codes for noncoherent channels", Sponsored by grants from Nationcal Science Foundation and National Aeronautics and Space Administration Lewis Research Center.

[14] G. L. Stuber, "Soft-limiter receivers for coded DS/DPSK systems," IEEE Trans. Commun, pp. 46 - 53, Jan. 1990.

[15] Y. T. Su, "Decoding metrics for slow frequency-hopped DPSK systems," in IEE Proc. Communications, Speech and Vision, vol. 139, Issue 5, pp. 525-532, Oct. 1992.